New Observations of North-American Intraplate Dynamic Seismic Triggering and Prevailing Conditions

Vivian Tang[1,1], Kevin Chao[1,1], and Suzan van der Lee[1,1]

[1]Northwestern University

November 30, 2022

Abstract

To facilitate identification of conditions that lead to the dynamic triggering of seismic events as catalogs of these events keep growing, we applied a machine-learning algorithm (decision tree) to a published data set of known instances of dynamically triggered seismic tremor in central California. To investigate the possible universality of our findings and to further test the algorithm, we also applied it to new observations, presented here, of potentially dynamically triggered seismic activity in three intraplate regions: Raton Basin (CO), Yellowstone, and central Utah. We report potential tremor or local earthquake signals from here during the propagation of surface waves from the 2012 Mw 8.6 Sumatra earthquake. These surface waves also triggered seismic activity along the western boundary of the North American plate and did not trigger seismic activity in the central and eastern USA. We report additional potential dynamic triggering in the three aforementioned intraplate regions from an investigation of seismograms from 37 additional large earthquakes, recorded between 2004 to 2017. Our findings show that transient stresses generated by surface waves from large earthquakes and arriving from favorable directions generally lead to triggered tremor in seismically, volcanically, and hydrothermally active regions like central California and possibly Yellowstone. These stresses do not appear to be decisive factors for the potentially dynamically triggered local earthquakes reported for the Raton Basin and central Utah, while surface waves' incidence angles do appear to be important there.

New Observations of North-American Intraplate Dynamic Seismic Triggering and Prevailing Conditions

Vivian Tang[1], Kevin Chao[1,2], and Suzan van der Lee[1,2]

[1]Department of Earth and Planetary Sciences, Northwestern University, Evanston, IL 60208

2 Northwestern Institute on Complex Systems, Northwestern University, Evanston, IL 60208

Corresponding author: Vivian Tang; Department of Earth and Planetary Sciences, Northwestern University, Evanston, IL 60208; Phone: +1-847-467-2467; Email: vivian@earth.northwestern.edu

Abstract

We systematically searched USArray seismograms for intraplate tremor and earthquakes that were dynamically triggered by the 2012 M_w8.6 Sumatra earthquake. We confirm triggered seismic activity along the western boundary of the North America and note the absence of triggered seismicity east of the Rocky Mountains. We newly observed dynamically triggered tremor near the Yellowstone hotspot, Wyoming, and triggered earthquakes in the Raton Basin and in central Utah. We then identified additional triggered events for each of these three locations by investigating seismograms recorded between 2001 to 2017. To advance our understanding and identification of the conditions that lead to dynamic triggering of seismic events, we applied a machine-learning algorithm (decision tree) to these three data sets as well as a published data set of known instances of triggered seismic tremor in central California. The algorithm found that dynamic stress estimates from teleseismic surface waves indeed appear to be a deciding factor in triggering tremor, though

may be secondary to the back azimuth from which the surface waves arrive. Our findings confirm that transient stresses generated by surface waves from strong earthquakes arriving from favorable directions can lead to triggered tectonic tremor in seismically active regions, such as central California and Yellowstone. These stresses do not appear to be deciding factors for the potentially dynamically triggered earthquakes in the Raton Basin and central Utah, while back azimuth does appear to be a deciding factor.

Key Points:

1. Dynamic triggering appears limited to seismically active regions, including intraplate regions Yellowstone, Colorado, and Utah.
2. Machine learning and visualization identify surface waves' back-azimuth as a decisive factor for dynamic triggering.
3. Peak stress is not deccisive for earthquake triggering and thresholds for triggering tremor vary regionally.

1. Introduction

Surface waves of large magnitude earthquakes ($M_w \geq 7.0$) can dynamically trigger subtle seismic events such as small earthquakes ($M_w \leq 3.0$) [*Prejean et al.*, 2004] and tectonic tremor [*Peng and Gomberg*, 2010] (Figure 1) thousands of kilometers away from the epicenter of the large-magnitude earthquakes. Signals from triggered earthquakes look just like signals from small local earthquakes and have significant *P* and *S* wave energy at high frequencies (greater than 5 Hz). For the purposes of this paper, triggered earthquake signals have the distinction that they occur during the arrival of surface waves, and have a statistical

probably of occurring during that window of less than 2%. Because we do not know for sure whether a local earthquake was dynamically or statically triggered, we refer to them as potentially triggered earthquakes. Signals from triggered tremor have significant frequency content between 2 to 8 Hz and bursts of triggered tremor occur during the strongest surface waves and can last for 5 to 30 minutes. The tremor usually looks like a series of bursts, which are modulated with the surface wave periodicity. With these criteria, a systematic survey of triggered seismic events can be conducted. Dynamic triggering of seismic events that advance slip on a local fault has been reported for stress perturbations of a mere 1~2 kPa, [*Peng and Gomberg*, 2010; *Brodsky and van der Elst*, 2014]. As triggered seismic events might occur only while the cumulative stress at a fault approaches its pre-slip state, a quantitative observation of triggered seismic events may provide useful information on the state of stress on the fault. Other reasons to study triggered seismic events include gathering information and insight on triggering and nucleation processes and mechanics in general.

Triggered tremor and triggered earthquakes have been observed at most plate boundaries and major faulting systems. Along the west coast of North America, many studies have reported dynamic triggering of earthquakes [*Velasco et al.*, 2008; *Aiken and Peng*, 2014; *Brodsky and van der Elst*, 2014; *Hill and Prejean*, 2015] and tremor [*Gomberg et al.*, 2008; *Peng et al.*, 2009; *Rubinstein et al.*, 2009; *Chao et al.*, 2012; *Gomberg and Prejean*, 2013; *Aiken and Peng*, 2014], but few studies searched for triggered seismic events in the continental interior of the United States [*Prejean et al.*, 2004; *Freed*, 2005; *van der Elst et al.*, 2013; *Velasco et al.*, 2016]. Within the interior of North America, the geothermally, volcanically, and seismically active region around Yellowstone National Park experienced dynamic triggering following the 2002 Denali earthquake [*Husen et al.*, 2004], as did the

Wasatch Fault zone in Utah [*Pankow et al.*, 2004]. Bockholt et al. (2014) searched for tectonic tremor in northern Tennessee around the Reelfoot Fault and found neither triggered nor ambient tremor. Previous studies have used automatic approaches for detecting triggered seismicity in the conterminous United States with USArray [e.g., *Cerda et al*., 2011; *Linville et al.*, 2014; *Velasco et al.*, 2016]. Velasco et al. (2016) found triggered earthquakes in Texas and the Coso region in California following the 2011 M_w9.0 Tohoku and the 2010 M_w8.8 Chile earthquakes, respectively. Nevertheless, Velasco et al. (2016) conclude that their deterministic detection algorithm significantly assists in data reduction but does not clearly identify dynamically triggered events.

With rapidly increasing volumes of data, geoscientists are turning to algorithms developed by the computer science community to solve geoscience problems [*Ramirez and Meyer*, 2011]. A dense seismic networks can provide a rich dataset for one earthquake to search for triggered seismic events, but a reasonably trained graduate student still needs over one month to process and thoroughly examine the recorded seismograms for potentially dynamically triggered events. Machine-learning algorithms can help extract meaningful and particular seismic signals from a big dataset [*Ramirez and Meyer*, 2011; *Lecun et al.*, 2015; *Tang et al.*, 2020].

In this study, we explore how machine-learning algorithms might facilitate the identification and quantification of triggering parameters and thresholds and search for triggered seismic events in the conterminous United States. To confirm whether the triggering of tectonic tremor is highly correlated with the dynamic stress generated by teleseismic surface waves, we apply a machine-learning algorithm, a decision-tree algorithm, to a known dataset of triggered tremor reported in California [*Chao et al.*, 2012] In addition, we search

for triggered tremor and triggered earthquakes in the conterminous United States following the 2012 Mw8.6 Sumatra earthquake and adapt the decision-tree algorithm to test the validation of stress-relative triggering threshold. In the following sections, we first introduce the decision-tree algorithm and the test results in California. Next, we show our examination results of newly found triggered seismic events in intraplate North-America. Finally, we discuss whether the dynamic stress is a critical factor for triggered tremor and triggered earthquakes.

2. Data and Methods: identification of potentially triggered seismic events

2.1 USArray data processing

The USArray (http://www.usarray.org) consists of a Transportable Array (TA) and a Flexible Array (FA), belonging to EarthScope. The TA has been operating since 2004, translating from west to east across the United States at a snail's pace before making a leap to Alaska, where it is currently deployed. The TA, equipped with three-component broadband stations separated by an approximate 70 km, is a large-scale seismic network. The FA consists of similar broadband stations that were deployed in smaller regions in more flexible geometries for limited durations by individual research teams. Here we included data from USArray and other permanent and temporary seismic networks that were recording in the US during the first decade of EarthScope (See "*Acknowledgements and Data*" for details).

For data processing, we downloaded all seismic waveforms from the IRIS (Incorporated Research Institutions for Seismology) Data Management System (DMS) (see "*Acknowledgements and Data*" for details). The downloaded waveforms start 60 minutes before and end 180 minutes after the origin times of selected large earthquakes. Waveforms

were examined in CrazyTremor (section 2.3) and those without signals of interest were removed. The remaining waveforms were converted to ground velocity, by deconvolving with the instrument response, and rotated to radial, transverse and vertical components. The waveforms were filtered with a 2-8 Hz band-pass filter when searching for triggered tremor or a 5 Hz high-pass filter when searching for triggered earthquakes.

2.2 Criteria for identifying triggered tremor and triggered earthquakes

To identify triggered tremor, we use the following criteria [*Chao and Yu*, 2018]: (1) tremor occurs during the arrivals of Love and Rayleigh waves, (2) tremor has dominant frequencies between 2 and 8 Hz; (3) tremor is represented by multiple apparent bursts, which are modulated by the surface waves (Figure 1b); (4) the tremor is either recorded by at least two stations within a 50 km of epicentral distance [*Chao et al.*, 2019] or has been activated by at least two large teleseismic earthquakes.

For searching for triggered earthquakes [*Aiken and Peng*, 2014], we consider an event as triggered earthquake if: (1) the earthquake occurs during the arrivals of Love and Rayleigh waves, (2) the earthquake signal has dominant frequencies over 5 Hz; (3) the earthquake signal shows clear P- and S-waves; (4) no significant background seismic activities within 24 hours before the examined time window; (5) the signals come from local earthquakes rather than teleseismic aftershocks.

Although triggered events have occurred during the arrival of body waves [*Hill et al.*, 2013; *Kundu et al.*, 2016] and major-arc Rayleigh waves [*Peng et al.*, 2011], we only focus on triggered events during the arrivals of Love and Rayleigh waves.

2.3 Initial identification with the CrazyTremor package

Initial separation of waveforms with signals of interest from those without such signals was carried out using Matlab program CrazyTremor [*Chao and Yu*, 2018], which was designed specifically for searching for dynamically triggered tremor and earthquakes. After loading SAC files into the CrazyTremor GUI (Figure 2), all seismograms were filtered (either 2-8 Hz band-passed or 5 Hz high-passed) and compared with surface waves in the broad-band seismogram. The three components of each seismograms were examined at same time and viewed as time series, envelopes, and/or spectrograms, to assist in the identification of station with triggered signals. Next, we used the tagging function of CrazyTremor to reject stations with no triggered signals and only kept stations with potentially triggered events. Finally, we grouped the filtered seismograms with CrazyTremor by increasing distance from the teleseismic earthquake, to confirm that the triggered events come from a local event.

3. Results

3.1 Observations of potentially triggered seismic events following the 2012 M_w8.6 Sumatra earthquake

The 11 April 2012 M_w8.6 Sumatra earthquake is the largest magnitude strike-slip earthquake to date [*Meng et al.*, 2012] (Table 1) and it generated large-amplitude and long-duration surface waves, which are considered ideal for dynamic triggering [*Peng and Gomberg*, 2010; *Hill*, 2012; *Bansal et al.*, 2016, 2018; *Chao and Obara*, 2016; *Johnson and Bürgmann*, 2016; *Kundu et al.*, 2016; *Chao and Yu*, 2018; Van der Elst et al., 2013; Castro et al., 2015]. Therefore, we searched for potentially dynamically triggered intraplate seismic events during the passage of surface waves from the 11 April 2012 M_w8.6 Sumatra earthquake.

We first visually examined radial, transverse and vertical components of 1,021

seismograms of the 2012 Sumatra earthquake (Figure 3), using CrazyTremor [*Chao and Yu*, 2018]. We examined seismograms from many stations simultaneously, to find events recorded by more than one station. After initial visual inspection, we rejected 617 seismograms because they exhibited either no high-frequency energy in the surface wave window or contained data gaps, calibrations, mass centering, or glitches.

Next, we carefully inspected the surface-wave window of the remaining 404 candidate seismograms for this earthquake in one or more frequency bands (i.e., 2-8 Hz band-passed or 5 Hz high-passed filter), using Seismic Analysis Code (SAC) [*Goldstein et al.*, 2005]. We identified signals as triggered earthquakes if they showed, for example, a relatively sudden onset and a pattern of possible *P* and *S* arrivals from a local earthquake. We identified signals as triggered tremor if the signals grew and waned more gradually in strength and appeared, for example, somewhat modulated by the large earthquake's long-period surface waves. Of these seismograms, 44 candidates remained that were most likely to contain observable recordings of dynamically triggered events. The rest of seismograms contain some type of high-frequency signal or noise in the surface window that neither qualified as tremor nor as earthquake. Thirty-three out of these 44 candidates were observed along the western plate boundary [*Castro et al.*, 2015 and *Castro et al.*, 2017], where triggered events had also been observed for other earthquakes [*Peng et al.*, 2009].

3.2 Quantifying triggered seismic events (background seismicity)

From the remaining eleven candidates of potentially newly discovered dynamic triggering, we rejected a further five, based on suspected instrument behavior (more details in the supplement material) or on the frequent occurrence of similar signals before and after the

surface wave window (Figure S1a) in regions that are seismically relatively quiescent, which indicated that these events were unlikely to be natural earthquakes and had a high probability of being randomly coincidental with the large earthquake's surface waves. The six remaining signals represent new detections (Figure 3) of dynamically triggered tremor sources in Yellowstone (H17A station), and dynamically triggered earthquake sources in Utah (SRU station) and Colorado (SDCO station, T25A station, Q24A station and S22A station). *Van der Elst* (2013) had previously reported triggered earthquakes from the 27 February 2010 M_w8.8 Chile earthquake, the 11 March 2011 Mw9.1 Tohoku earthquake and the 11 April 2012 M_w8.6 Sumatra earthquake at station T25A. We selected SDCO station as a long-term representative station to use for searching for additional dynamically triggered seismicity in Colorado.

4. Testing of triggering threshold with a decision-tree algorithm

4.1 Theory of decision-tree

The decision tree is a machine-learning algorithm and a powerful prediction method [*Mitchell*, 1997; *Saxena*, 2017]. In decision analysis, a decision tree can be applied to learn deciding factors leading to decisions or other binary outcomes, for example which seismograms are most likely to have recorded dynamically triggered local seismic events, based on a set of attribute values. The set of examples (seismograms) is $\boldsymbol{X}$ which are observed in a particular seismic station:

$$X = \{\overrightarrow{x_1}, \ldots \overrightarrow{x_n}\}$$

Each example (seismogram) $\boldsymbol{x}$ is represented by a $\boldsymbol{k}$-tuple of parameters (attribute values $\boldsymbol{a}$).

$$\vec{x}=< a_1, \dots, a_k >$$

As described below, the algorithm first selects the attribute that corresponds most decisively with one of the two groups of seismograms: those that recorded triggered events and those that did not. It then places this "best" attribute and its decisive threshold at the root (top panel of Figure S11) of the tree, split the training set into subsets according to the attribute value, and then calculate the next most decisive attribute for each subset. We repeat the procedure to classify the dataset. While running the decision tree algorithm, we assume the following: the entire training set is considered the root at the beginning; the order of attributes placed in the tree is done by using a "entropy" minimization-based statistical approach [*Mitchell*, 1997]; and the dataset is suitable for categorization.

The concept for attribute selection in our study is to calculate the "entropy" S value as follows:

$$S = \sum_{x\in} -P(x)logP(x)$$

Entropy represents the level of chaos for the decision tree system, and P is the probability $\frac{\boldsymbol{x}}{\boldsymbol{X}}$ for each tree system, $\boldsymbol{X}$ is the set of examples. For a binary classification problem with two classes, positive and negative class, x indicates the number of each class. We take the $\boldsymbol{X}$ examples to be the training samples, build the decision tree based on each attribute, and then choose the attribute with the smallest entropy value as the best attribute. If all examples are positive or all are negative then the entropy will be zero. If half of examples are positive and half of them are negative, the entropy will be one.

4.2 Training dataset: triggered tremor catalog in California

To test this decision-tree algorithm, we first applied a simplified training data set that

228 included triggered tremor observations in Parkfield in central California following 42
229 teleseismic earthquakes between 2001 and 2010 (Table S1 of Chao et al., 2012, see “Data
230 and Resource” for detail table link). We used a triggered tremor catalog observed in northern
231 California around the Calaveras Fault, central California near the Parkfield-Cholame section
232 of the San Andreas Fault, and southern California near the San Jacinto Fault [*Chao et al.*,
233 2012; *Kano et al.*, 2018]. This catalog includes the examination results from 42 triggering
234 earthquakes between 2001 and 2010. There are 12 tremor-triggering events observed in
235 central California and only one tremor-triggering events observed in northern and southern
236 California. The catalog also included the maximum apparent dynamic stress observed in each
237 region for both triggering and non-triggering events.
238
239 **4.3 Results of Decision-tree Algorithm**
240 As previous studies [*Chao et al.*, 2012; *Peng at al.*, 2009] have suggested that station
241 PKD can be used as an indicator station for determining the existence of triggered tremor, we
242 assigned dynamic stresses estimated from the vertical and transverse components of
243 seismograms recorded at station PKD as attributes. Also, we included other potentially
244 relevant and likely irrelevant attributes: the solid-earth tide, back azimuth, and whether it is
245 day or night, and provide them to the decision-tree algorithm. The final results (simplified in
246 Figure 10) show that vertical-component dynamic stress estimate is the most decisive factor
247 as to whether seismograms in the California dataset contain triggered tremor. The threshold
248 value for the dynamic stress above which triggering occurred is about 3.33 kPa.
249
250 **5. Expansion to data from other large earthquakes**

5.1 Additional data selection

To investigate whether or not the 2012 M_w8.6 Sumatra earthquake was the only earthquake that triggered seismic events in the three aforementioned locations, we searched for additional strong earthquakes in the ANSS (Advanced National Seismic System, see "*Acknowledgements and Data*" for the webpage link) global earthquake catalog. We selected earthquakes with moment magnitude (M_w) greater than 7.0, an event depth less than 100 km, and at least 10° away [*Chao and Obara,* 2016] from the pertinent locations. Between 2004 and 2017, 158 earthquakes matched these criteria. For each location, we estimated the surface wave displacement amplitudes generated by the large earthquake's surface waves using a magnitude-distance relationship [*Chao et al.*, 2013], and selected only those earthquakes with estimated amplitudes greater than a few *mm*, which corresponds to at least one stress tensor component exceeding 10 kPa. This left 37 additional candidate earthquakes (Figure 4) for triggering local seismic events in the three identified locations. With some of these earthquakes being recorded by a subset of the stations (H17A, SRU, and SDCO) at the three locations, we obtained 97 additional seismograms to examine. Within these 97 seismograms and for 15 of the 38 earthquakes, we found 15 possible dynamically triggered events recorded within the surface-wave arrival window (Figures S2-S9), loosely defined by bounding group velocity limits of 5 and 2 km/s. We also examined seismograms at nearby stations for each newly found potentially triggered event. Using data from nearby stations we were able to locate 12 of these 15 local events.

In addition, we estimate the dominant dynamic shear stress imposed by a strong surface wave by approximating the deviatoric shear strain as the one half of surface-wave ground velocity divided by the surface wave's group velocity, then multiplying it with twice the shear

modulus:

$$\sigma = \mu \dot{u}/U$$

,where μ is shear modulus and $\dot{u}/U$ is the deviatoric strain, which is computed by the surface-wave ground velocity ($\dot{u}$) and the surface wave's group velocity (U) [*Chao and Obara*, 2016].

Using μ = 35 GPa as a representative shear modulus for the crust and U = 3.5 km/s as a representative average group velocity, we estimate the peak shear stress in kPa to equal $10^4 \times A$, where A is the peak ground velocity in m/s. Figure 5 shows the inferred apparent dynamic shear stress estimated from the vertical and transverse seismogram components versus back-azimuths.

In the following sub-sections, we discuss these new detections (Figure 6, 7 and 8) in detail.

5.2 Observations of triggered tremor in Yellowstone (H17A station)

The H17A station in Yellowstone National Park recorded tremor potentially triggered by four earthquakes (Table 3): #8, #20 (Figure 8a), #21 and #37 earthquake (Figure 8c). The peak dynamic stresses inferred from both the vertical and transverse components for these four instances of dynamic triggering were greater than 5 kPa (Figure 5, Table S1).

Station H17A is located within the Yellowstone Caldera, right by West Thumb Caldera. Yellowstone is an active super volcano [*Huang et al.*, 2015], and thus it is not surprising that local earthquakes occur frequently (Figure 9). We also found triggered tremor at one nearby station, B944, from the 20 March 2012 M_w7.5 Mexico earthquake (Figure S5).

296 **5.3 Observations of triggered earthquakes in central Utah (SRU station)**

297 Seismograms from the SRU station in Utah, show recordings of twelve local
298 earthquakes that were potentially triggered by the following twelve large earthquakes (Table
299 4): #8, #9, #10, #13, #14, #15, #21, #23, #24, #26, #30, and #34.

300 The inferred peak dynamic stresses for these recordings range from less than 3.3 kPa to
301 7.2 kPa (Table S1), and do not differ in an obvious way from peak dynamic stresses inferred
302 from surface waves that did not trigger a local earthquake.

303 Station SRU is in central Utah, about 100 km east of a roughly north-south oriented belt
304 of seismicity and about 50 km south of a roughly east-west oriented lineament of seismicity.
305 The strongest local earthquake in this area had a magnitude of 4.2 during the period spanned by
306 our data (https://earthquake.usgs.gov/). However, not far from SRU lies the Wasatch Fault,
307 where dynamic triggering of earthquakes has been reported following the 2002 Denali fault
308 earthquake [*Pankow et al.*, 2004].

309 We searched for potentially triggered local earthquake signals in data from earthquake
310 #21 recorded at relatively nearby stations within about 100 km from SRU station (Table 4).
311 We observed signals from this local earthquake at seven nearby stations: TMU, CVRU, BCE,
312 PNSU, ROA, DCM and ARGU, and located its epicenter using CrazyTremor (Figure 6).

313 We also found a probable triggered earthquake in data from earthquake #9 recorded at
314 SRU and 7 nearby stations (P14A, Q14A, P16A, Q16A, P17A, R17A and Q18A) and located
315 the source of this local earthquake from these 8 records (Figures 9 and S2). Probable
316 triggered earthquake signals were recorded at 7 nearby stations (TMU, Q18A, Q16A, P18A,
317 ROA, P17A, DBD) from earthquake #10, at station Q16A from earthquake #15, and at
318 station TMU from earthquake #23. Furthermore, we found probable triggered earthquakes

and located the epicenter of this earthquake using 14 nearby stations (station Q16A, P18A, S18A, P19A, O19A, DUG, Q20A, R20A, O20A, S20A, N20A, N21A, N22A and R24A) around the station SRU from #13 (Figure 9). A potentially triggered earthquake was recorded by SRU, ARGU, DCM and PNSU station from the #24. Earthquake #14 potentially triggered another local earthquake that was recorded not only at station SRU but also at nearby stations CCUT, Q16A and R11A (Figure S4), and its epicenter is shown in Figure 9.

Surface waves from earthquakes #8, #26 and #34 may also have triggered local earthquakes but these were observed only in data from station SRU. Because these signals were not observed at other stations we did not select these data for training our decision tree algorithm. ARGU, DCM and EMU station recorded a possible triggered earthquake from earthquake #31 but station SRU did not record it and therefore it also was not included in the decision tree we built for SRU-recorded signals of potentially triggered events.

5.4 Observations of triggered earthquakes in Colorado (SDCO station)

Two local earthquakes recorded by station SDCO in Colorado were possibly dynamically triggered by the following three possible teleseismic earthquakes: #21, #23 (Figure 8b) and #24. The inferred peak dynamic stresses for these recordings range from less than 1.5 kPa to more than 7.0 kPa (Table S1), and do not differ in an obvious way from peak dynamic stresses inferred from surface waves that did not trigger a local earthquake.

Station SDCO is at the eastern edge of the Colorado Plateau and by the northern branch of the Rio Grande Rift. The region around SDCO is not particularly seismically active. The closest known earthquakes to SDCO are a pair of 2003 M~3 earthquakes, 25 km SE of the station (https://earthquake.usgs.gov/). However, the station is about 80 km northwest of the

342 Raton Basin, which has experienced an increase in seismic activity and wastewater injection
343 over the past two decades [*Nakai et al.*, 2017; *Yeck et al.*, 2016].

344 We observed potentially triggered earthquakes from 6 nearby station T25A, Q24A,
345 S22A, XTOCO, HGTCO and LVTCO from earthquake #21 and applied CrazyTremor to
346 locate the epicenter of this local earthquake (Figure 7) from these 7 records. We also found
347 that the local earthquake that was potentially triggered by #23 was also observed at 16
348 stations (station T25A, S22A, Q24A, ANMO, TASL, TASM, KSCO, MVCO, ISCO, AMTX,
349 MSTX, CBKS, OGNE, SRU, MNTX and WMOK) near station SDCO. We located the
350 epicenter of this earthquake to be in the Raton Basin (Figure 9). Surface waves from
351 earthquake #24 may also have triggered a local earthquake but it was observed only in data
352 from station SDCO. Because these signals were not observed at other stations we did not
353 select this data for training our decision tree algorithm.

354 For earthquake #21, the local earthquake signals in Utah (Figure 6) arrive about 5,430
355 seconds after the origin time of earthquake #21 while in Colorado (Figure 7) they arrive
356 about 200 seconds later, which indicates that the surface waves from earthquake #21
357 triggered a local earthquake earlier in Utah than in Colorado. Figure 3 shows that these
358 surface waves propagated roughly from northwest to southeast in the western US and would
359 have indeed needed about 200 s to travel from station SRU in Utah to station SDCO in
360 Colorado. This evidence suggests that these earthquakes in Utah and Colorado are
361 dynamically triggered rather than coincident earthquakes.

362

363 **6. Application of the Decision Tree Algorithm to the quantification of triggering**
364 **potential**

We applied our decision-tree algorithm to the events described in section 5: local earthquakes and tremor likely triggered (Table S1) by surface waves from some of the 38 teleseismic earthquakes. The results of this application are summarized in Figure 11, with the entire decision tree provided in Figure S13.

The results show that for both Yellowstone and station SDCO in Colorado (Figure 11 a and c), the back azimuth appears to be the most-decisive attribute in triggering local tremor and earthquakes, respectively. In other words, surface waves associated with local events at these two locations all arrive at back azimuths within a range of about 16°.

For triggering tremor in the Yellowstone region the second-most decisive factor appears to be the peak stress inferred from Love waves ("transverse stress"). If the peak "transverse stress" exceeds a threshold of 10 kPa tremor is triggered in four of the eight cases within the optimal back-azimuth range, while tremor is not triggered for the other four cases when the peak "transverse stress" is below this threshold (Figure 11a).

In addition, peak stresses do *not* appear to be important for earthquake triggering near station SDCO (Figure 11c), and appear to be anti-correlated with triggering near station SRU in Utah, where local earthquakes are associated with "transverse stresses" *below* 2.5 kPa (Figure 11b). In short, the local earthquakes we reported in both Utah and Colorado are *not* primarily associated with peak stress values.

At this point it has become clear that estimates of peak stress are important factors for triggering *tremor* in both the Yellowstone region and Central California (Figures. 10a and 11a), which is consistent with much of the literature on dynamic triggering.

At the same time our analysis of likely dynamically triggered local *earthquakes* in Colorado and Utah shows that these earthquakes occur independently of peak stress values.

7. Discussion

In a search for dynamically triggered events in all of the conterminous United States, we confirmed the notion that seismic events are predominantly triggered in regions of high tectonic and seismic activity (the westernmost boundary of the North American tectonic plate). Within USArray data from earthquake #21 (2012 M_w8.6 Sumatra), we did not find signals of triggered seismic events in the Archean, Proterozoic and Paleozoic parts of North America east of the Rocky Mountains. Consistent with these end-member findings of lots of triggered activity along the west coast and little in tectonically stable North America, we found a small number of seismic events, triggered by earthquake #21 and other teleseismic earthquakes, in three locations in the western-US interior that are less seismically active than the westernmost plate boundary. Specifically, we newly detected four potentially triggered tremor bursts in Yellowstone, twelve potentially triggered earthquakes in Utah, as well as three potentially triggered earthquakes in Colorado from an examination of seismograms from 38 large teleseismic earthquakes (Table 2).

Our decision-tree algorithm trained with triggered tremor dataset in central California, found a peak stress, estimates from Rayleigh waves, of 3.3 kPa as a triggering threshold there. This is less than the typically used empirical value of 5 kPa but more than the lowest stresses for which triggering has been reported [*Peng and Gomberg*, 2010; *Brodsky and van der Elst*, 2014]. Hill et al. (2013) suggest that, specifically for the San Andreas Fault near Parkfield, CA, Rayleigh waves modulate tremor via pore pressure fluctuations, but that the fault slip associated with the tremor is caused by SH and Love waves polarized largely perpendicular or parallel to the San Andreas Fault. Figure 10 confirms this notion and shows that the back

azimuths for earthquakes that triggered tremor are either somewhat aligned or at right angles with the San Andreas Fault's strike. Our finding expands on this by suggesting that, if vertical-component stresses indeed govern pore pressure, then pore pressure may be the second most important factor, after back-azimuth (*i.e.* fault orientation), controlling whether such tremor and associated slip can take place. Our decision tree skipped the back-azimuth attribute for California because the attribute was defined only for two-lobed patterns (with a 180° period rather than a 90° period).

Dynamically triggered events are hard to detect in raw seismograms, their identification can be negatively affected by various types of noise, instrumental quirks or adjustments, glitches, data gaps, or might coincide with rather than be triggered by large earthquakes' surface waves. For example, upon first examination, we observed two candidate triggered earthquakes in Minnesota after earthquake #21 (Figure S1). A subsequent closer inspection did not reject the candidate triggered events since the signals shared characteristics with triggered earthquake signals. However, after inspection of hours and days of seismograms before and after the earthquake, we rejected both candidates because a multitude of similar signals, possibly from anthropogenic events, implied a high likelihood for one of these events coinciding with the earthquake's surface waves by chance. Through the use of visual inspection in addition to timing- and frequency-based selection criteria for these seismic phenomena, our search yielded numerous false positives, indicating the challenge posed by moving from ad-hoc observations of dynamic triggering to a systematic search that also includes a catalog of teleseismic events that did not dynamically trigger other events, even when large stress variations were supplied.

Table 2 presents the 38 teleseismic earthquakes in our study, 12 of which produced

potentially triggered events in the three study regions. In addition to these 12, about 20 of the 38 earthquakes produced peak dynamic stresses over 1.5 kPa (Table S1), but were not included in the analysis because they either did not trigger earthquakes or tremor (such as in 6 instances at SDCO stations) or triggered events whose signals were hidden by other signals or noise (about 15 other cases). For example, earthquake #18 (2011 M_w9.1 Tohoku) was immediately followed by a series of strong aftershocks whose seismic waves could have obscured signals form potentially triggered local earthquakes or tremor.

Our observations, analyses, and decision-tree confirm the greater likelihood for triggered *tremor* from high dynamic stress surface waves as reported in the literature. Our results also indicate that triggered *earthquakes* are *not* positively correlated with high dynamic stress surface waves, in agreement with [*Wang et al*., 2018]. On the contrary, our analysis shows that back-azimuth *is* an important decisive factor, for both earthquakes and tremor, in whether dynamic triggering occurs or not. This is the case in at least three (Yellowstone, Colorado, and central California) of the four regions analyzed here, and back-azimuth likely also plays a role in the fourth region (Utah), for example in a four-lobed pattern (Figure 5) similar to California.

A large number of surface waves (Table S1) with favorable back-azimuths (Figure 5), have been observed to not be associated with triggering, which argues for future multi-factor analyses, including stresses values at depth within the crust, all components of the dynamic stress tensors from simultaneously arriving Love and Rayleigh waves, and how dynamic stress tensors translate to stress quantities that matter to faulting.

The application of a decision-tree machine-learning algorithm to an existing and a new data set of likely triggered events has provided us with several insights:

1. Back-azimuth appears to be a decisive factor in whether surface waves can trigger local tremor or earthquakes,
2. A quantitative threshold of 3.3 kPa for peak “vertical” dynamic stresses from Rayleigh waves that appear to trigger tremor in central California,
3. A quantitative threshold of 10 kPa for peak “transverse” dynamic stresses from Love waves that appear to trigger tremor in Yellowstone,
4. Peak dynamic stress values do not appear to be important for triggering local earthquakes, at least in Utah and Colorado,
5. The exact mechanism of dynamically triggering seismic events is still unknown, and while back-azimuth and peak dynamic stress estimates are important, other attributes likely also play a role (for example, stress at depth, full stress tensors, and interaction with particular faults).

8. Conclusions

Reports about dynamically triggered seismic events are regularly published in the professional literature [*Freed*, 2005; *Gonzalez-Huizar et al.*, 2012; *Aiken and Peng*, 2014; *Yao et al.*, 2015; *Johnson et al.*, 2015; *Bansal et al.*, 2016; *Bansal et al.*, 2018; *Opris et al.*, 2018; *Prejean and Hill*, 2018; *Wang et al.*, 2018], yet many aspects about the physical mechanisms leading to such triggering remain elusive. Documenting instances of dynamically triggered seismic events and the conditions under which they occur and not occur provide us with data to illuminate some of these aspects. In this paper we approached this challenge from multiple different perspectives:

1. We used a decision tree algorithm and rose diagrams (Figures 5, 10, and 11) to determine that the back azimuth of surface waves is a decisive factor in dynamic triggering.
2. Our decision tree algorithm further showed that dynamic stresses from teleseismic surface waves are, as expected by practitioners, the most important attribute for triggering tectonic tremor in central California and Yellowstone. Out of 42 world-wide earthquakes with magnitudes over 7.5, all of those with Rayleigh waves generating over 3.3 kPa in peak stress changes in central California triggered tectonic tremor. Out of 38 world-wide earthquakes with magnitudes over 7.0, all of those with Love waves generating over 10 kPa in peak stress changes in Yellowstone triggered tectonic tremor.
3. We examined each seismogram recorded anywhere in the US (*sans* Alaska and Hawaii) of the 11 April 2012 M_w8.6 Sumatra earthquake as to whether a dynamically triggered seismic event was recorded. We did not find any such events east of the Rocky Mountains but we found several dozens of records of dynamically triggered events along the western edge of the North American Plate, which have previously been reported in the literature. Newly, we detected likely dynamically triggered tremor in the Yellowstone hotspot region, and a dynamically triggered earthquake in each of central Utah and southeastern Colorado, near the Raton Basin.
4. Our experiments with automating such detections have so far been thwarted by instrumental quirks, mass centerings, calibrations, possible non-linear behavior, data gaps, high noise, industrial and other human activity, and a suite of other types of noise or signals. Furthermore, we detected a significant number of “false triggers” during the examinations discussed in this paper. A “false trigger” is a seismic record that looks like a record of

tremor or an earthquake but is rather a record of one of the above-listed non-seismic signals.

5. We examined seismograms from 37 additional worldwide earthquakes with magnitudes over 7.0 that were recorded near Yellowstone, central Utah, and the Raton Basin. This examination identified one more dynamically triggered earthquake in the Raton Basin, three more instances of dynamically triggered tremor in Yellowstone, and four more dynamically triggered earthquakes in Utah.
6. Application of the aforementioned decision tree further revealed that peak dynamic stresses estimated from teleseismic surface waves does not appear to correlate with whether or not a local earthquake is triggered.

Acknowledgements and Data

This research is funded by the Integrated Data-Driven Discovery in Geophysical and Astrophysical Sciences (IDEAS) program under National Science Foundation grant NSF-NRT 1450006 and by Northwestern University's Data Scholar Program of the Data Science Initiative (DSI). K. Chao was also supported by the Finite Earth Research Support Program from the Northwestern Institute on Complex Systems. We are grateful to Bryan Pardo for accommodating VT in his machine-learning course and for enlightening discussions and to Boris Rösler for stimulating discussions.

All seismic data were downloaded through the IRIS Wilber 3 system (http://ds.iris.edu/wilber3/find_event), including the following seismic networks (http://ds.iris.edu/mda): USArray (2003), ANZA (1982), BDSN (1980), SCSN (1926), SPREE (2011), GSN-IRIS/IDA (1986), GSN-IRIS/USGS (1988), NSN (1971), UOPNSN

(1990), USNSN (1990), Utah Network (1962), PNSN (1963), OIINK (2011), FAME (2007), SIEDCAR (2008), IOPS (2011), CAFE (2006), FACES (2007), NE-NV BB/Stanford (2010), SESAME (2010) and MAGIC (2013).

The ANSS (Advanced National Seismic System) earthquake catalog can be accessed at https://earthquake.usgs.gov/data/comcat/. Solid tide data can be accessed at http://geodesyworld.github.io/SOFTS/solid.htm.

References

Professional papers

Aki, K., Fehler, M., and Das, S. (1977), Source mechanism of volcanic tremor: fluid-driven crack models and their application to the 1963 Kilauea eruption, *Journal of Volcanology and Geothermal Research*, *2*(3), 259–287, doi:10.1016/0377-0273(77)90003-8.

Aiken, C., and Z. Peng (2014), Dynamic triggering of microearthquakes in three geothermal/volcanic regions of California, *J. Geophys. Res. Earth*, *119*, 6992–7009, doi:10.1002/ 2014JB011218.

Bansal, A. R., D. Yao, Z. Peng, and D. Sianipar (2016), Isolated regions of remote triggering in South/Southeast Asia following the 2012 Mw8.6 Indian Ocean earthquake, *Geophys. Res. Lett.*, *43*(20), 10,654-10,662, doi:10.1002/2016GL069955.

Bansal, A. R., N. P. Rao, Z. Peng, D. Shashidhar, and X. Meng (2018), Remote Triggering in the Koyna-Warna Reservoir-Induced Seismic Zone, Western India, *J. Geophys. Res. Solid Earth*, *123*(3), 2318–2331, doi:10.1002/2017JB014563.

Brodsky, E. E., and N. J. van der Elst (2014), The Uses of Dynamic Earthquake Triggering, *Annu. Rev. Earth Planet. Sci.*, *42*(1), 317–339,

547 doi:10.1146/annurev-earth-060313-054648.
548 Chao, K., Peng, Z., Gonzalez- Huizar, H., Aiken, C., Enescu, B., Kao, H., Vaelasco A.A.,
549 Obara, K. and T. Matsuzawa (2013). A global search for triggered tremor following the
550 2011 M w 9.0 Tohoku earthquake. *Bulletin of the Seismological Society of*
551 *America*, *103*(2B), 1551-1571.
552 Chao, K., and K. Obara (2016), Triggered tectonic tremor in various types of fault systems of
553 Japan following the 2012 M_w 8.6 Sumatra earthquake, *J. Geophys. Res. Solid Earth*,
554 *121*(1), 170–187, doi:10.1002/2015JB012566.
555 Chao, K., and C. Yu (2018), A MATLAB GUI for Examining Triggered Tremor: A Case
556 Study in New Zealand, *Seismol. Res. Lett.*, doi:10.1785/0220180057.
557 Chao, K., Z. Peng, A. Fabian, and L. Ojha (2012), Comparisons of triggered tremor in
558 California, *Bull. Seismol. Soc. Am.*, *102*(2), 900–908, doi:10.1785/0120110151.
559 Chao, K., Z. Peng, Y.-J. Hsu, K. Obara, C. Wu, K.-E. Ching, S. van der Lee, H.-C. Pu, P.-L.
560 Leu, and A. Wech (2017), Temporal variation of tectonic tremor activity in southern
561 Taiwan around the 2010 ML6.4 Jiashian earthquake, *J. Geophys. Res. Solid Earth*,
562 *122*(7), 5417–5434, doi:10.1002/2016JB013925.
563 Chao, K., Z. Peng, W. B. Frank, G. A. Prieto, and K. Obara (2019), Isolated Triggered Tremor
564 Spots in South America and Implications for Global Tremor Activity, *Seismol. Res. Lett.*,
565 *90*(5), 1726–1739, doi:10.1785/0220190009.
566 Castro, R. R., González- Huízar, H., Ramón Zúñiga, F., Wong, V. M., & Velasco, A. A.
567 (2015). Delayed dynamic triggered seismicity in northern Baja California, México caused
568 by large and remote earthquakes. *Bulletin of the Seismological Society of America*, *105*(4),
569 1825-1835, doi:10.1785/0120140310.

570 Castro, R. R., Clayton, R., Hauksson, E., & Stock, J. (2017). Observations of remotely
571 triggered seismicity in Salton Sea and Coso geothermal regions, Southern California,
572 USA, after big (MW> 7.8) teleseismic earthquakes. *Geofísica internacional*, *56*(3),
573 269-286.
574 Delaney, P. T., and A. E. Gartner (1997), Physical processes of shallow mafic dike
575 emplacement near the San Rafael Swell, Utah, *Geol. Soc. Am. Bull.*, *109*(9), 1177–1192,
576 doi:10.1130/0016-7606(1997)109<1177:PPOSMD>2.3.CO;2.
577 van der Elst, N. J., H. M. Savage, K. M. Keranen, and G. A. Abers (2013), Enhanced Remote
578 Earthquake Triggering at Fluid-Injection Sites in the Midwestern United States, *Science*
579 *(80-.).*, *341*(September), 1380–1385, doi:10.1126/science.1238948.
580 Freed, A. M. (2005), Earthquake Triggering by Static, Dynamic, and Postseismic Stress
581 Transfer, *Annu. Rev. Earth Planet. Sci.*, *33*(1), 335–367,
582 doi:10.1146/annurev.earth.33.092203.122505.
583 Goldstein, P. A. U. L., and A. Snoke (2005), SAC availability for the IRIS
584 community. *Incorporated Research Institutions for Seismology Newsletter*, *7*
585 (UCRL-JRNL-211140).
586 Gomberg, J., and S. Prejean (2013), Triggered tremor sweet spots in Alaska, *J. Geophys. Res.*
587 *Earth*, *118*(12), 6203–6218, doi:10.1002/2013JB010273.
588 Gomberg, J., J. L. Rubinstein, and Z. Peng (2008), Widespread triggering of nonvolcanic
589 tremor in California, *Science (80-.).*, *319*, 173, doi:10.1126/science.1149164.
590 Gonzalez-Huizar, H., A. A. Velasco, Z. Peng, and R. Castro (2012), Remote triggered
591 seismicity caused by the 2011, M9.0 Tohoku, Japan earthquake, *Geophys. Res. Lett*,
592 *L10302*, doi:10.1029/2012GL051015.

593 Hill, D. P., and S. G. Prejean (2015), Dynamic Triggering, in *Treatise on Geophysics*, vol. 4,
594 pp. 273–304, Elsevier.
595 Hill, D. P., Z. Peng, D. R. Shelly, and C. Aiken (2013), S-Wave Triggering of Tremor beneath
596 the Parkfield, California, Section of the San Andreas Fault by the 2011 Tohoku, Japan,
597 Earthquake: Observations and Theory, *Bull. Seismol. Soc. Am.*, *103*(2B), 1541–1550,
598 doi:10.1785/0120120114.
599 Huang, H. H., F. C. Lin, B. Schmandt, J. Farrell, R. B. Smith, and V. C. Tsai (2015), The
600 Yellowstone magmatic system from the mantle plume to the upper crust, *Science (80-.).*,
601 *348*(6236), 773–776, doi:10.1126/science.aaa5648.
602 Husen, S., S. Wiemer, and R. B. Smith (2004), Remotely Triggered Seismicity in the
603 Yellowstone National Park Region by the 2002 Mw 7.9 Denali Fault Earthquake, Alaska,
604 *Bull. Seismol. Soc. Am.*, *94*(6B), S317–S331, doi:10.1785/0120040617.
605 Johnson, C. W., R. Bürgmann, and F. F. Pollitz (2015), Rare dynamic triggering of remote *M*
606 $\geq$5.5 earthquakes from global catalog analysis, *J. Geophys. Res. Solid Earth*, *120*(3),
607 1748–1761, doi:10.1002/2014JB011788.
608 Kano, M. et al. (2018), Development of a Slow Earthquake Database, *Seismol. Res. Lett.*,
609 *89*(4), 1566–1575, doi:10.1785/0220180021.
610 Linville, L., Pankow, K., Kilb, D., & Velasco, A. (2014). Exploring remote earthquake
611 triggering potential across EarthScopes' Transportable Array through frequency domain
612 array visualization. *Journal of Geophysical Research: Solid Earth*, *119*(12), 8950-8963.
613 Lecun, Y., Y. Bengio, and G. Hinton (2015), Deep learning, *Nature*, *521*(7553), 436–444,
614 doi:10.1038/nature14539.
615 Milbert, D. (2015), Solid earth tide program: solid. Retrieved August 10, 2018, *from*

http//geodesyworld, github, io/SOFTS/solid.htm, written in fortran.

Mitchell, T. M. (Tom M. (1997), *Machine Learning*, 1st ed., McGraw-Hill.

Nakai, J. S., M. Weingarten, A. F. Sheehan, S. L. Bilek, and S. Ge (2017), A Possible Causative Mechanism of Raton Basin, New Mexico and Colorado Earthquakes Using Recent Seismicity Patterns and Pore Pressure Modeling, *J. Geophys. Res. Solid Earth*, *122*(10), 8051–8065, doi:10.1002/2017JB014415.

Opris, A., B. Enescu, Y. Yagi, and J. Zhuang (2018), Triggering and decay characteristics of dynamically activated seismicity in Southwest Japan, *Geophys. J. Int.*, *212*(2), 1010–1021, doi:10.1093/gji/ggx456.

Pankow, K. L., W. J. Arabasz, J. C. Pechmann, and S. J. Nava (2004), Triggered Seismicity in Utah from the 3 November 2002 Denali Fault Earthquake, *Bull. Seismol. Soc. Am.*, *94*(6B), S332–S347, doi:10.1785/0120040609.

Peng, Z., J. E. Vidale, A. G. Wech, R. M. Nadeau, and K. C. Creager (2009), Remote triggering of tremor along the San Andreas Fault in central California, *J. Geophys. Res.*, *114*(B00A06), doi:10.1029/2008JB006049.

Peng, Z., and J. Gomberg (2010), An integrated perspective of the continuum between earthquakes and slow-slip phenomena, *Nat. Geosci.*, *3*, 599–607, doi:10.1038/ngeo940.

Prejean, S. G., D. P. Hill, E. E. Brodsky, S. E. Hough, M. J. S. Johnston, S. D. Malone, D. H. Oppenheimer, A. M. Pitt, and K. B. Richards-Dinger (2004), Remotely triggered seismicity on the United States west coast following the Mw 7.9 Denali fault earthquake, *Bull. Seismol. Soc. Am.*, *94*(6B), S348–S359.

Prejean, S. G., and D. P. Hill (2018), The influence of tectonic environment on dynamic earthquake triggering: A review and case study on Alaskan volcanoes, *Tectonophysics*,

639 *745*, 293–304, doi:10.1016/J.TECTO.2018.08.007.
640 Ramirez, J., and F. G. Meyer (2011), Machine learning for seismic signal processing: Seismic
641 phase classification on a manifold, in *Proceedings - 10th International Conference on*
642 *Machine Learning and Applications, ICMLA 2011*, vol. 1, pp. 382–388.
643 Rubinstein, J. L., J. Gomberg, J. E. Vidale, A. G. Wech, H. Kao, K. C. Creager, and G.
644 Rogers (2009), Seismic wave triggering of nonvolcanic tremor, episodic tremor and slip,
645 and earthquakes on Vancouver Island, *J. Geophys. Res.*, *114*(B00A01),
646 doi:10.1029/2008JB005875.
647 Saxena, R. (2017), Building Decision Tree Algorithm, *Retrieved May 23, 2018, from*
648 *https//dataaspirant.com/2017/02/01/decision-treealgorithm-python-with-scikit-learn/.*
649 Tang, V., Seetharaman, P., Chao, K., Pardo, A. B. and S. van der Lee (2020), Automating the
650 Detection of Dynamically Triggered Earthquakes via a Deep Metric Learning Algorithm.
651 Seismological Redearch Letters, doi:10.1785/0220190165.
652 Velasco, A., S. Hernandez, and T. Parsons (2008), Global Ubiquity of Dynamic Earthquake
653 Triggering, *Nat. Geosci*, *1*, 375–379, doi:10.1038/ngeo204.
654 Velasco, A., R. Alfaro- Diaz, and D. Kilb (2016), A Time- Domain Detection Approach to
655 Identify Small Earthquakes within the Continental United States Recorded by the
656 USArray and Regional Networks, *Bull.*
657 Wang, B., Harrington, R. M., Liu, Y., Kao, H., & H. Yu (2019), Remote Dynamic Triggering
658 of Earthquakes in Three Unconventional Canadian Hydrocarbon Regions Based on a
659 Multiple- Station Matched- Filter Approach. *Bulletin of the Seismological Society of*
660 *America*, *109*(1), 372-386.
661 Yao, D., Z. Peng, and X. Meng (2015), Remotely triggered earthquakes in South-Central

Tibet following the 2004 Mw 9.1 Sumatra and 2005 Mw 8.6 Nias earthquakes, *Geophys. J. Int.*, *201*(2), 543–551, doi:10.1093/gji/ggv037.

Yeck, W. L., Weingarten, M., Benz, H. M., McNamara, D. E., Bergman, E. A., Herrmann, R. B., ... & Earle, P. S. (2016). Far- field pressurization likely caused one of the largest injection induced earthquakes by reactivating a large preexisting basement fault structure. *Geophysical Research Letters*, *43*(19), 10-198.

Data Sources

Albuquerque Seismological Laboratory (ASL)/USGS (1988), Global Seismograph Network - IRIS/USGS. International Federation of Digital Seismograph Networks. Dataset/Seismic Network, doi:10.7914/SN/IU.

Albuquerque Seismological Laboratory (ASL)/USGS (1990), United States National Seismic Network. International Federation of Digital Seismograph Networks. Dataset/Seismic Network, doi:10.7914/SN/US.

Brudzinski, M. and R. Allen (2007), Resolving structural control of episodic tremor and slip along the length of Cascadia. International Federation of Digital Seismograph Networks. Dataset/Seismic Network, doi:10.7914/SN/YW_2007.

California Institute of Technology and United States Geological Survey Pasadena (1926), Southern California Seismic Network. International Federation of Digital Seismograph Networks. Dataset/Seismic Network, doi:10.7914/SN/CI.

Fischer, K. M., Hawman, R. B. and L. S. Wagner (2010), Southeastern Suture of the Appalachian Margin Experiment. International Federation of Digital Seismograph Networks. Dataset/Seismic Network, doi:10.7914/SN/Z9_2010.

685 IRIS Transportable Array (2003), USArray Transportable Array. International Federation of
686 Digital Seismograph Networks. Dataset/Seismic Network, doi:10.7914/SN/TA.
687 Klemperer, S. and K. Miller (2010), Flexarray 3D Passive Seismic Imaging of Core-Complex
688 Extension in the Ruby Range Nevada. International Federation of Digital Seismograph
689 Networks. Dataset/Seismic Network, doi:10.7914/SN/YX_2010.
690 Levander, A. (2007), Seismic and Geodetic Investigations of Mendocino Triple Junction
691 Dynamics. International Federation of Digital Seismograph Networks. Dataset/Seismic
692 Network, doi:10.7914/SN/XQ_2007.
693 Long, M. and P. Wiita (2013), Mid-Atlantic Geophysical Integrat ive Collaboration.
694 International Federation of Digital Seismograph Networks. Dataset/Seismic Network,
695 doi:10.7914/SN/7A_2013.
696 Northern California Earthquake Data Center (2014). *Berkeley Digital Seismic Network*
697 *(BDSN)*. Northern California Earthquake Data Center, doi:10.7932/BDSN.
698 Malone, S., Creager, K., Rondenay, S., Melbourne, T. and G. Abers (2006), Collaborative
699 Research: Earthscope integrated investigations of Cascadia subduction zone tremor,
700 structure and process. International Federation of Digital Seismograph Networks.
701 Dataset/Seismic Network, doi:10.7914/SN/XU_2006.
702 Pulliam, J., Grand, S. and J. Sansom (2008), Seismic Investigation of Edge Driven
703 Convection Associated with the Rio Grande Rift. International Federation of Digital
704 Seismograph Networks. Dataset/Seismic Network, doi:10.7914/SN/XR_2008.
705 Pavlis, G. and H. Gilbert (2011), Ozark Illinois Indiana Kentucky (OIINK) Flexible Array
706 Experiment. International Federation of Digital Seismograph Networks. Dataset/Seismic
707 Network, doi:10.7914/SN/XO_2011.

Russo, R. (2011), Deformation and Magmatic Modification of a Steep Continental Margin, Western ID-Eastern OR. International Federation of Digital Seismograph Networks. Dataset/Seismic Network, doi:10.7914/SN/XT_2011.

University of Washington (1963): Pacific Northwest Seismic Network. International Federation of Digital Seismograph Networks. Dataset/Seismic Network, doi:10.7914/SN/UW.

University of Nevada, Reno (1971), Nevada Seismic Network. International Federation of Digital Seismograph Networks. Dataset/Seismic Network, doi:10.7914/SN/NN

UC San Diego (1982), ANZA Regional Network. International Federation of Digital Seismograph Networks. Dataset/Seismic Network. 10.7914/SN/AZ.

University of Oregon (1990), University of Oregon and Pacific Northwest Seismic Network. International Federation of Digital Seismograph Networks. Dataset/Seismic Network, doi:10.7914/SN/UO.

van der Lee, S., Wiens, D., Revenaugh, J., Frederiksen, A. and F. Darbyshire (2011), Superior Province Rifting Earthscope Experiment. International Federation of Digital Seismograph Networks. Dataset/Seismic Network, doi:10.7914/SN/XI_2011.

Figures

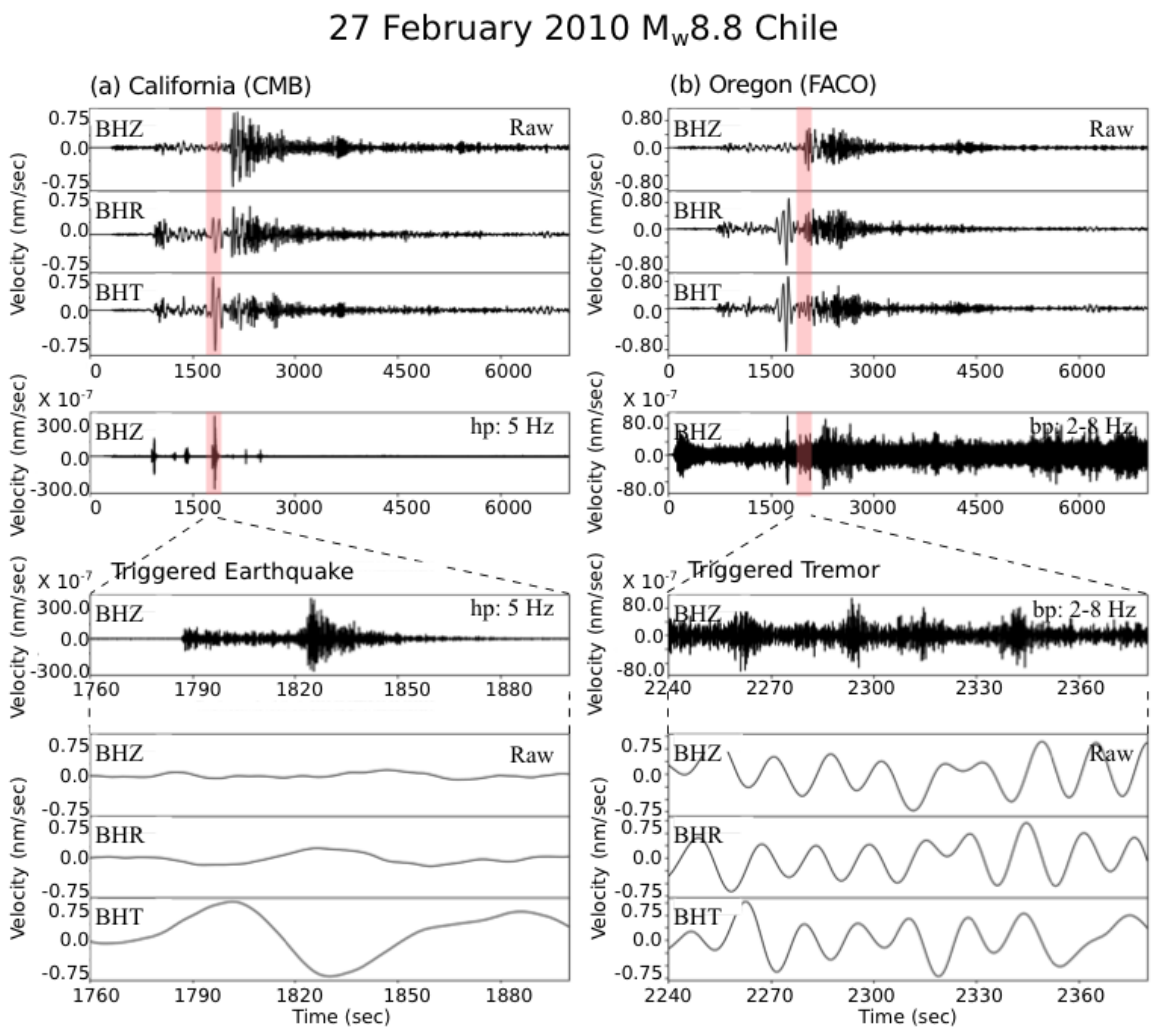

731

732 **Figure 1.** Examples of dynamic triggering of triggered earthquakes (a) and triggered tremor
733 (b) following the surface waves of the 27 February 2010 M_w8.8 Chile earthquake. Some of
734 the seismograms are high-pass filtered 5 Hz in order to identify the locally triggered
735 earthquakes. Thickness red line represents the enlarge window for observing the triggered
736 tremor and earthquake.

(a) Triggered earthqukake in Utah following the 2009/05/28 Mw7.3 event

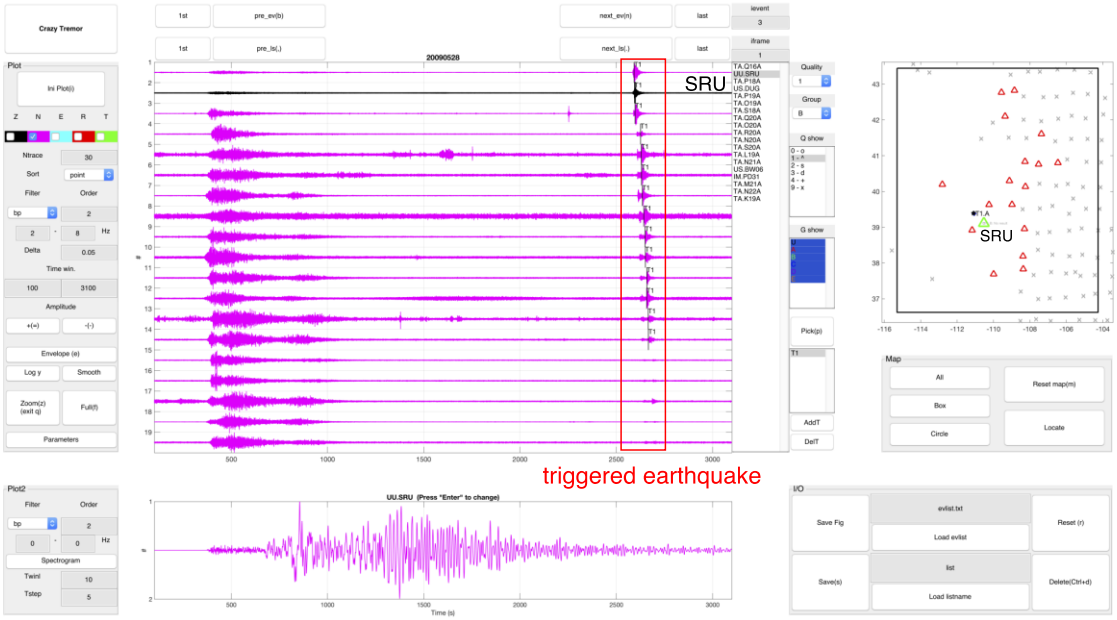

(b) Zoom-in seismograms of the triggered earthquake

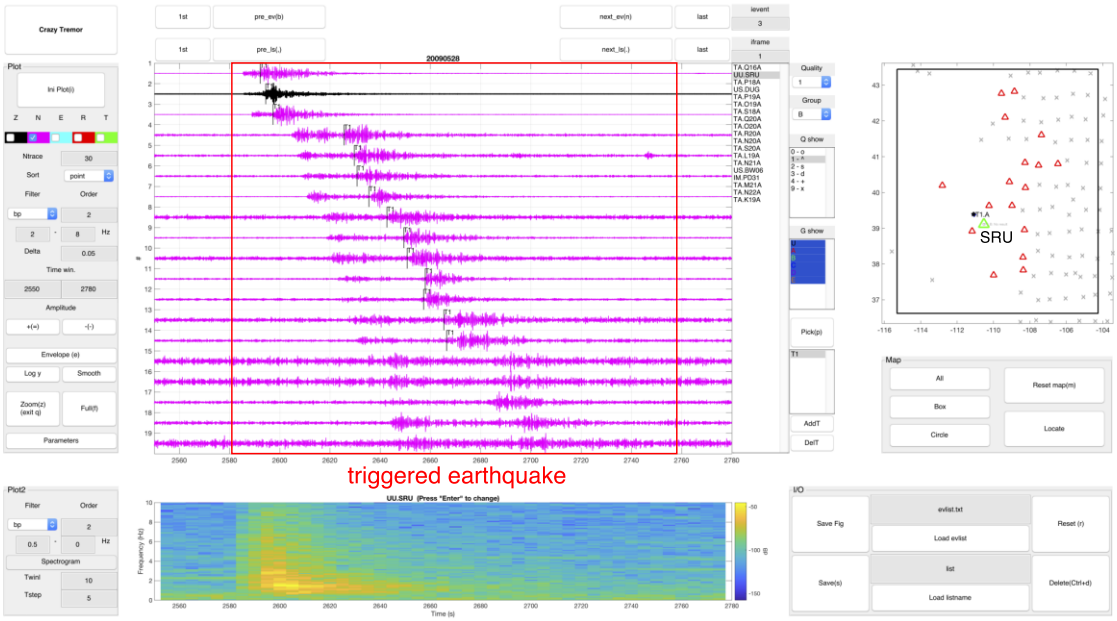

Figure 2. (a) Snapshot of CrazyTremor, a MATLAB GUI-based software package (Chao and Yu, 2018), shows triggered earthquake in Utah recorded by 19 USArray stations following the 28 May 2009 M_w7.3 Honduras earthquake. Triggered earthquakes appear on the 2–8 Hz band-pass filtered seismograms at ~2500 seconds. The bottom panel shows a

seismogram of station SRU (green triangle). (b) Zoom-in seismograms of triggered earthquakes. The bottom panel shows a spectrogram of one selected station SRU. Black star represents the source of the local earthquake.

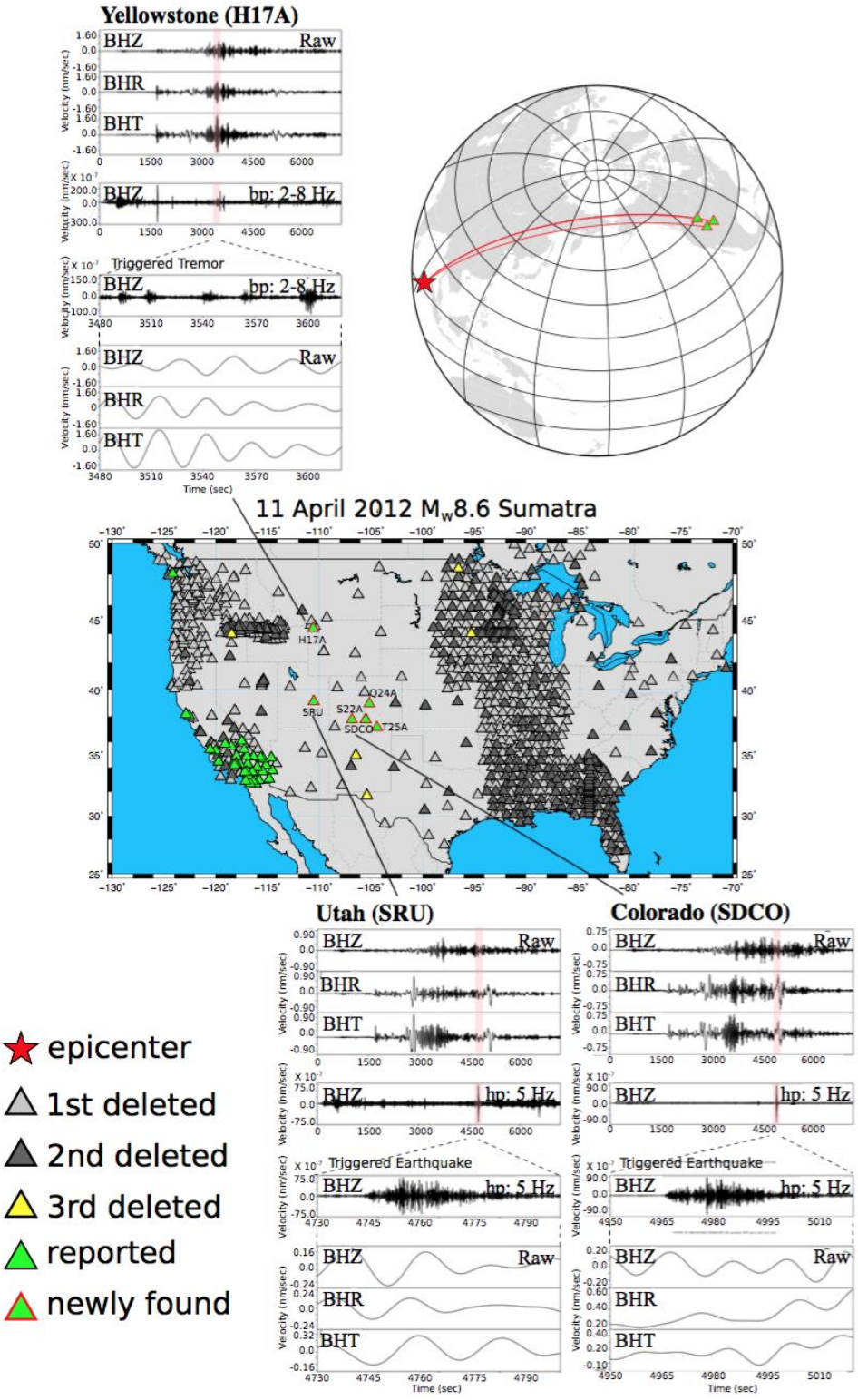

Figure 3. Sumatra earthquake and examined stations. Three-component seismogram panels show raw data (top), high-passed data, and data with enlarge window (bottom) for the newly found triggered tremor and triggered earthquakes. Thickness red line represents the enlarge window for observing the triggered tremor and earthquake.

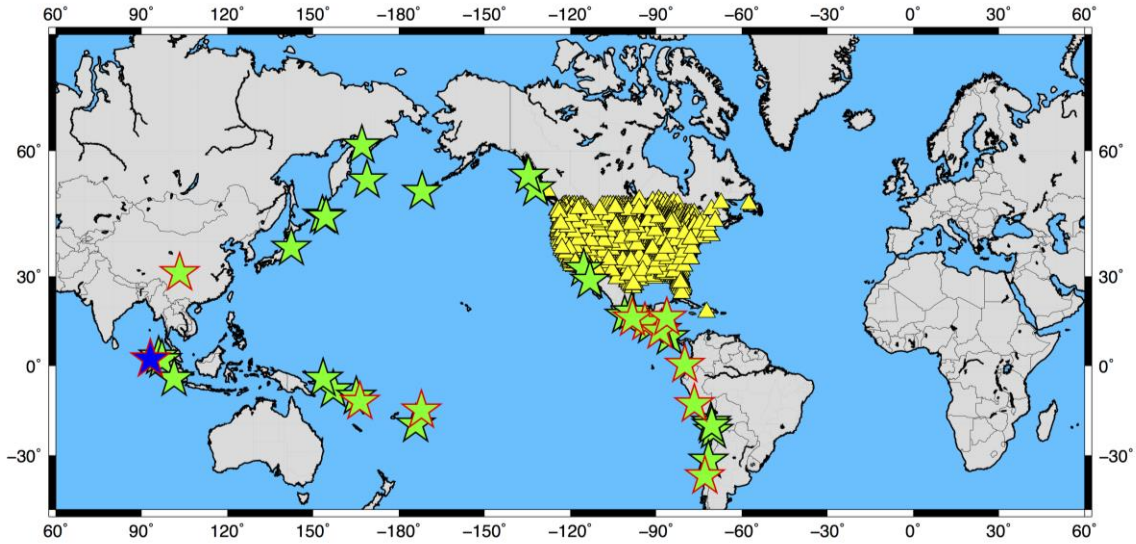

Figure 4. 38 triggering earthquakes (stars) and examined stations (yellow triangles) in this study. Blue star is the 2012 M_w8.6 Sumatra earthquake. We focused on examining only newly found triggered tremors and earthquakes in Yellowstone, Colorado and Utah. Stars with red frame indicate that we found triggered tremor or earthquake in Yellowstone, Colorado and Utah from the teleseismic earthquake.

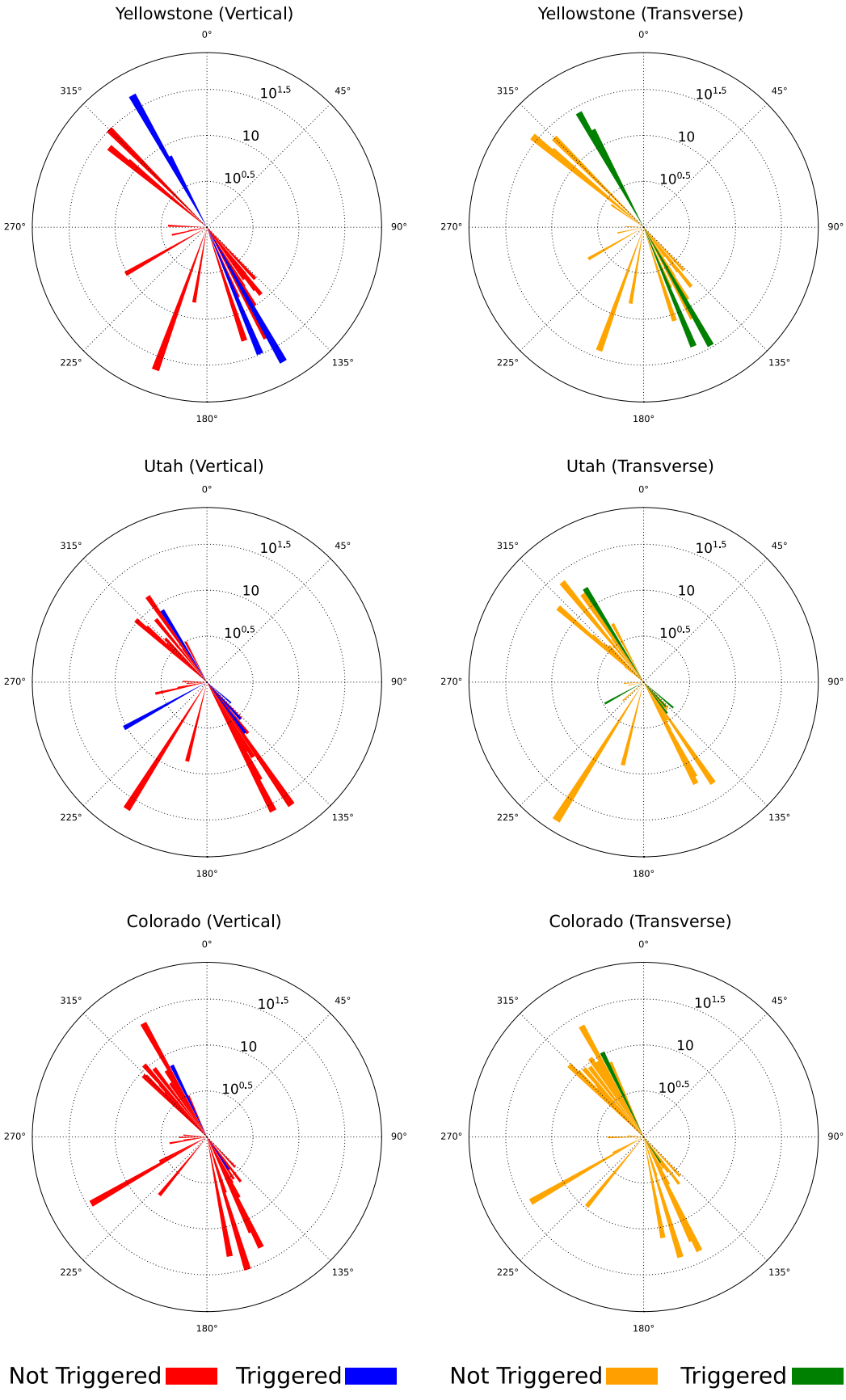
Yellowstone (Vertical)
Yellowstone (Transverse)
Utah (Vertical)
Utah (Transverse)
Colorado (Vertical)
Colorado (Transverse)
0°
45°
90°
135°
180°
225°
270°
315°
10
$10^{0.5}$
$10^{1.5}$
Not Triggered
Triggered
Not Triggered
Triggered

756

Figure 5. Triggered (blue bars: at the vertical component; green bars: at the transverse component) and no triggered events (red bars: at the vertical component; orange bars: at the transverse component) plotted vs. the dynamic stress proxy and the incidence angle (BAZ, back azimuth) at three stations (a-c) that recorded newly found triggered events during the surface waves. The length of the lines represents the value of the peak dynamic stress (kPa).

(a) Tirggered earthquake in Utah following the 2012/04/11 Mw8.6 event

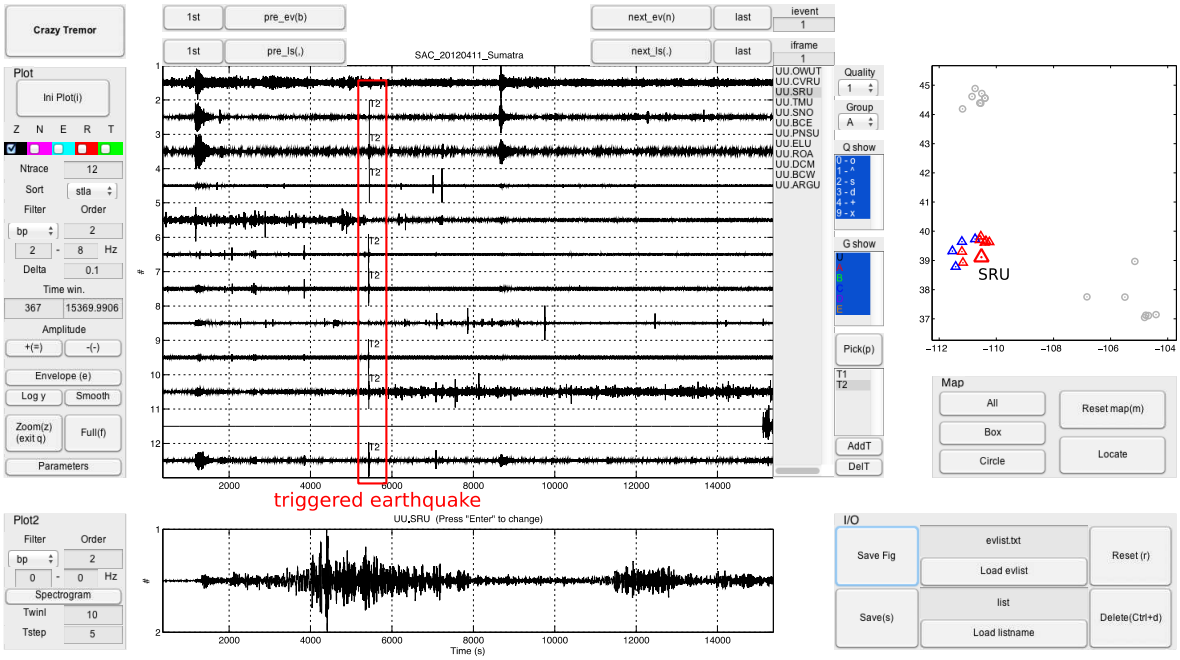

(b) Zoom-in seismograms of the triggered earthquake

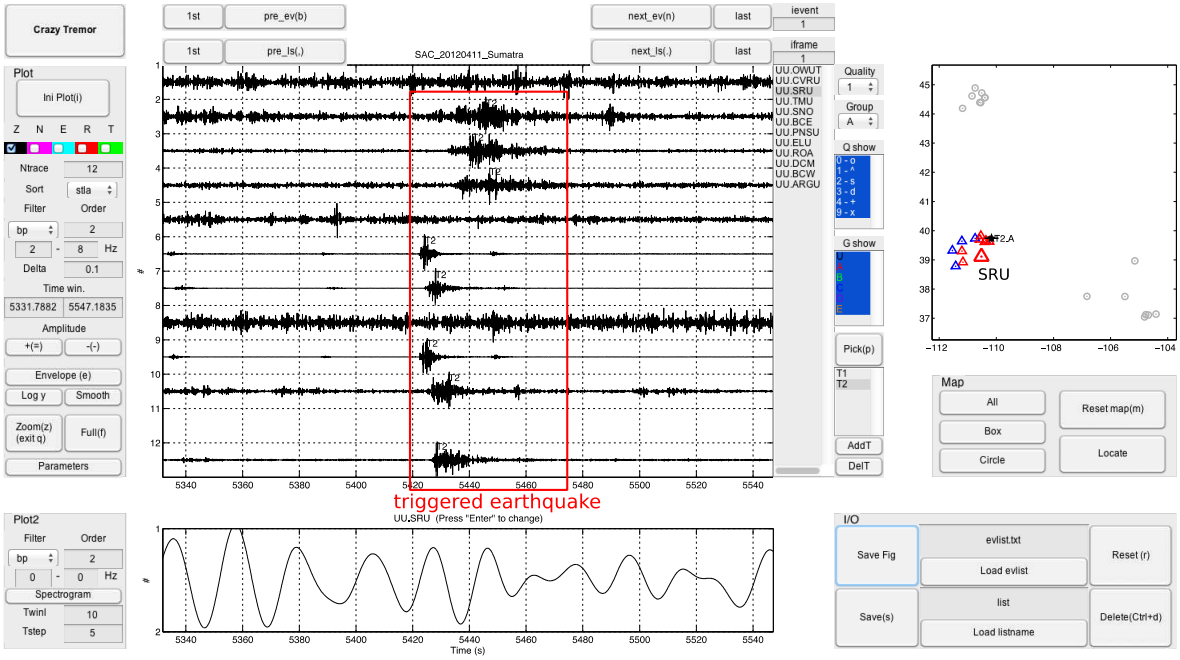

Figure 6. Seismograms of a triggered earthquake in central Utah (SRU station) and nearby stations following the 11 April 2012 Mw8.6 Sumatra earthquake. Blue represents stations did not record a clear triggered earthquake or no triggered earthquake. We only use red stations to locate the local source (black star).

(a) Triggered earthquake in Colorado following the 2012/04/11 Mw8.6 event

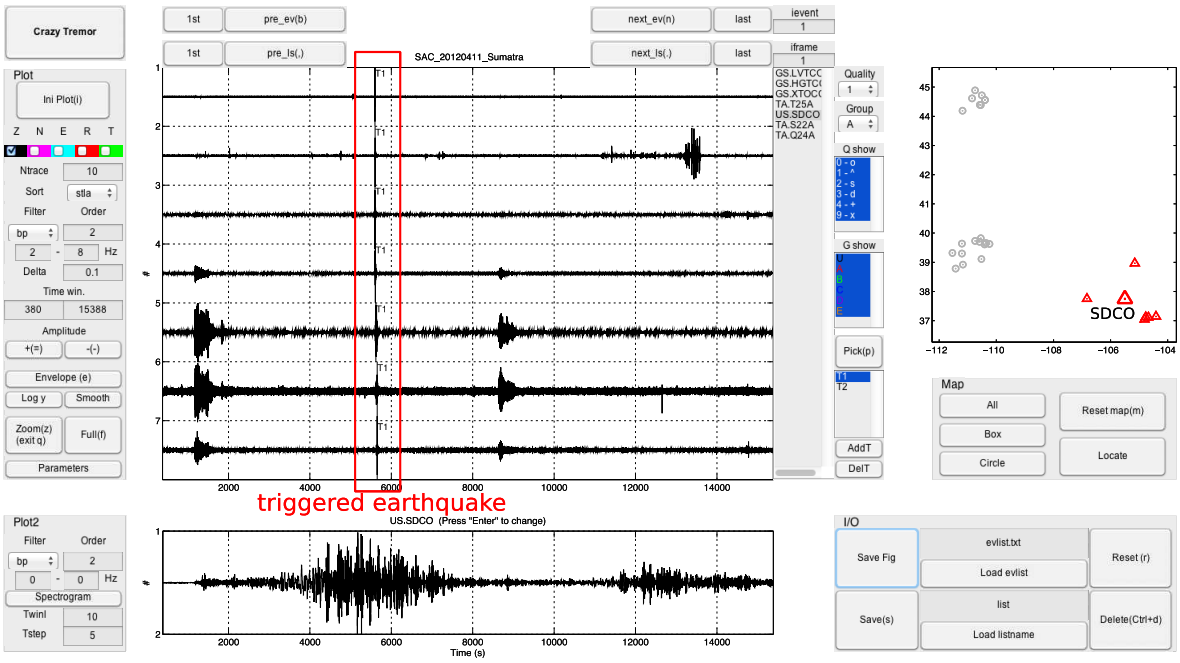

(b) Zoom-in siesmograms of the triggered earthquake

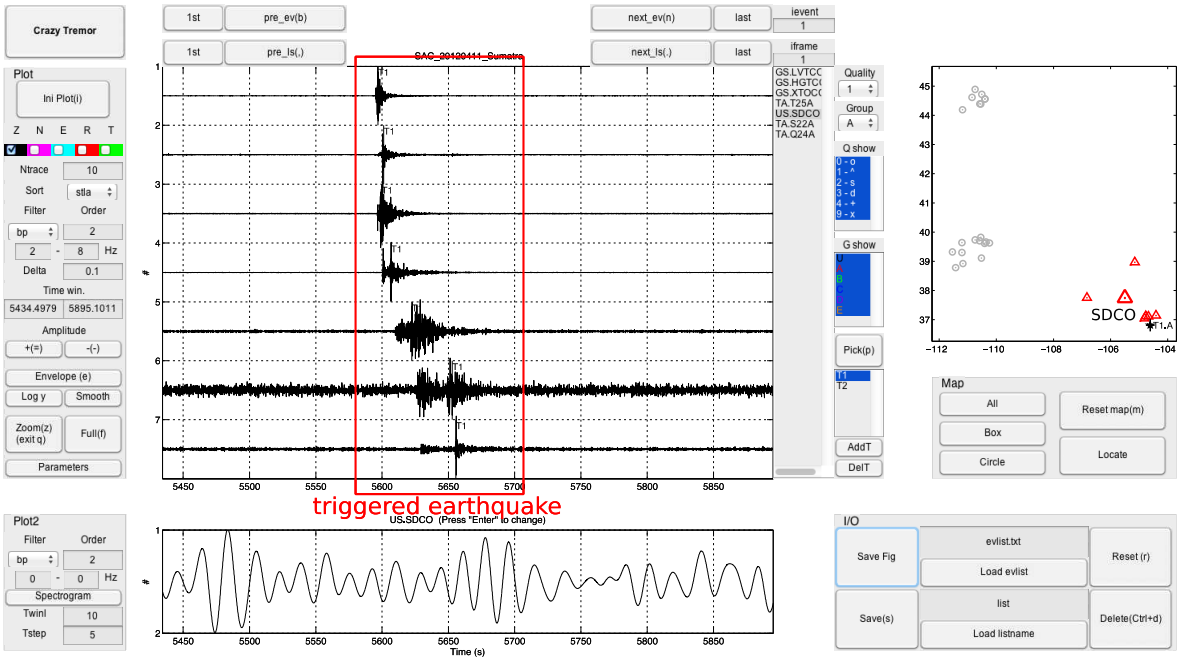

Figure 7. Seismograms of the triggered earthquake in Colorado (SDCO station) and nearby stations following the 11 April 2012 Mw8.6 Sumatra earthquake. Star represents the local source location.

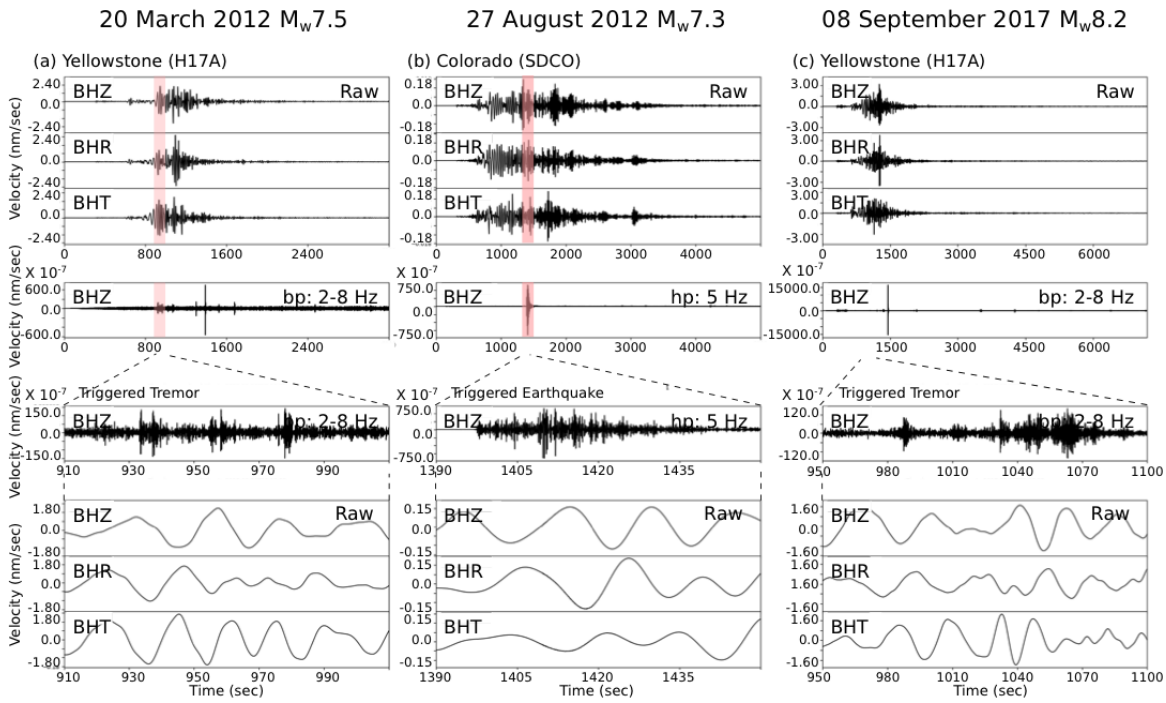

Figure 8. (a) and (c) Triggered tremor in Yellowstone (H17A station), but from the 20 March 2012 M_w7.5 Mexico earthquake and the 8 September 2017 M_w8.1 Mexico earthquake. (b) Triggered earthquake at the SDCO station, but from the 27 August 2012 M_w7.3 Nicaragua earthquake.

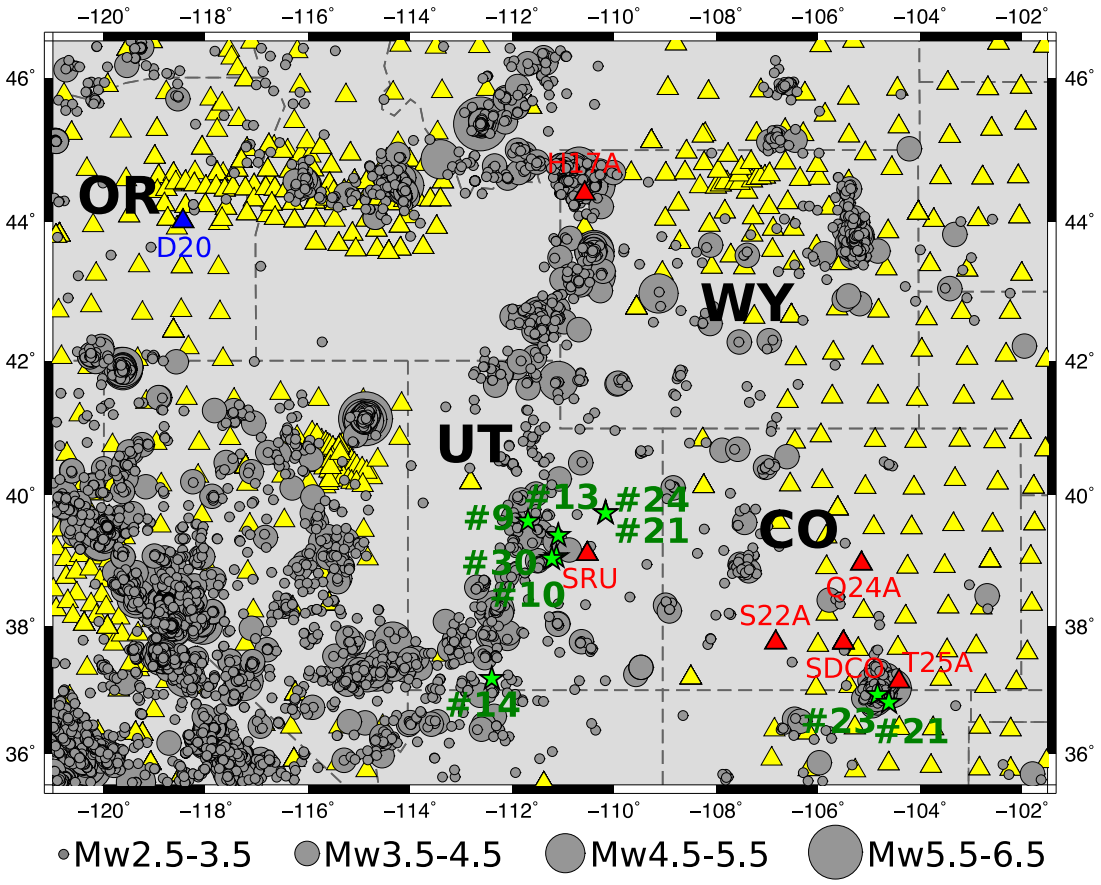

780

781 **Figure 9.** Seismic activities from 2004 to 2017 in Yellowstone, Utah, and Colorado. Size of
782 the gray circle depends on magnitude of the earthquake. The earthquake catalog can be
783 accessed at https://earthquake.usgs.gov/. Red triangles are our newly found stations; blue star
784 in Oregon is a negative example of potential triggered tremor. Green stars indicate the
785 triggered earthquakes locations following the teleseismic earthquakes in Table 2.

786

787

788

789

790

791

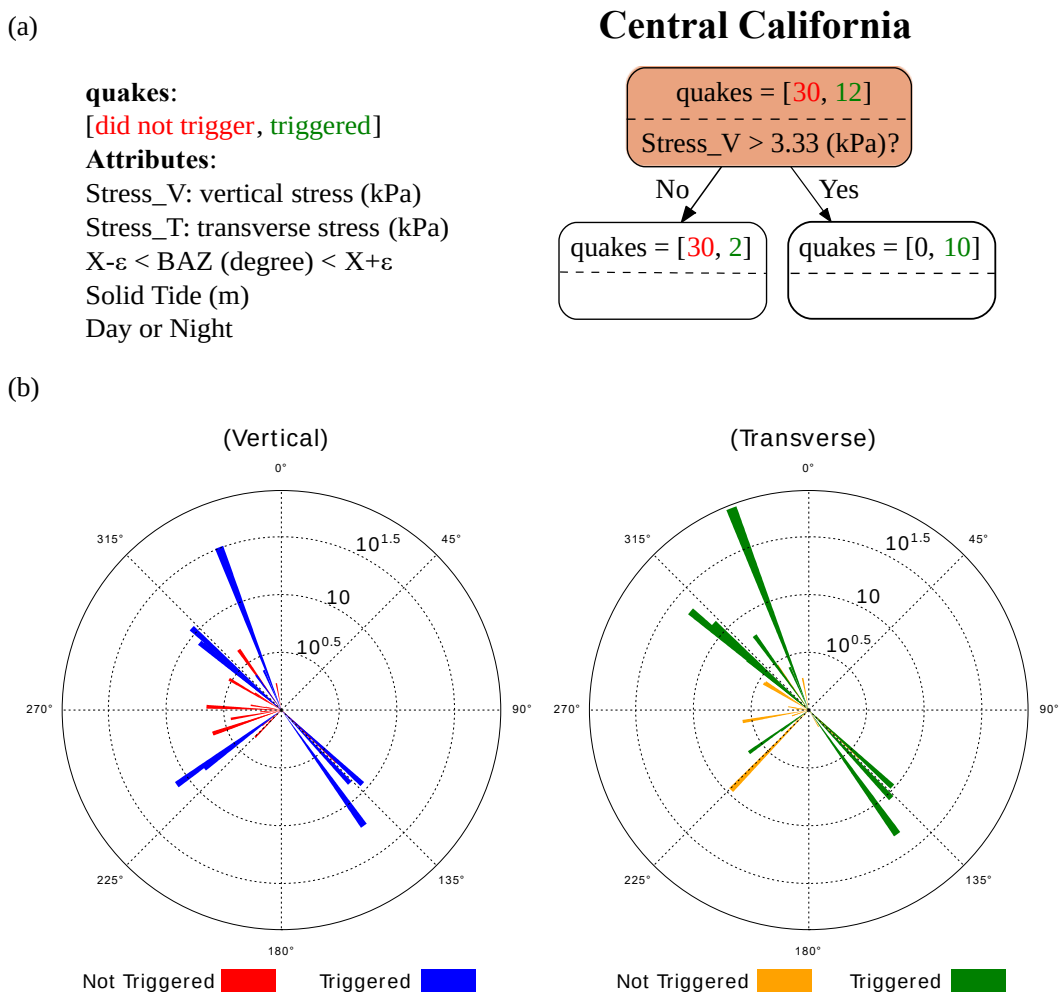

Figure 10. (a) We tested the decision-tree algorithm with the examination results of triggered tremor in central California (Chao et al., 2012). "Stress_V" ("vertical stress") and "Stress_T" ("transverse stress") represent observed dynamic stress at vertical and transverse components. "Solid tide" is computed with the open source code from Milbert et al. (2015). The "BAZ" is represented as the back azimuth, and $\boldsymbol{\varepsilon}$ represents the absolutely value of cosine of back azimuth subtract average a constant $\boldsymbol{X}$ due to the back azimuth is cyclic and has a 180° periodicity. $\boldsymbol{X}$ is represented as average back azimuths' value of triggered events, which is 123.76° (or 307.76°) in central California. "Day" is defined as the period between 6 am to 6 pm, local time, and "Night" is the complementary period. (b) Triggered (blue bars: at the vertical component; green bars: at the transverse component) and no triggered events (red

bars: at the vertical component; orange bars: at the transverse component) plotted vs. the dynamic stress proxy and the incidence angle (BAZ, back azimuth) at central California. The length of the lines represents the value of the vertical dynamic stress.

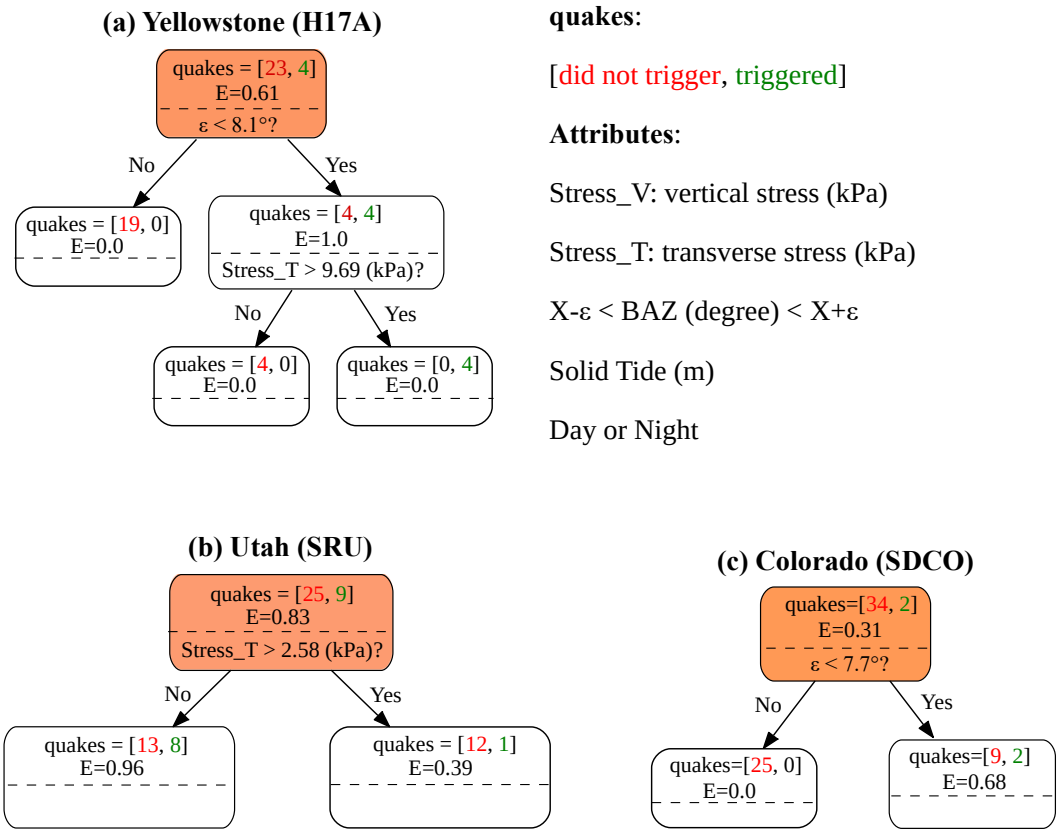

Figure 11. We tested the decision-tree algorithm with the examination results of triggered tremor in Yellowstone (a) and triggered earthquakes in Utah (b) and Colorado (c). X is 151.20° (or 331.2°), 122.13° (or 302.13°) and 148.74° (or 328.74°) in Yellowstone, Utah and Colorado respectively. Please read the supporting Figure S12 and S13 for complete decision-tree calculation.

Table 1. Strike-slip earthquakes with Mw>8 from 2001 to 2017 year.

Date	Longitude	Latitude	Depth	Mw
2004/12/23 14:59:30.9	161.25	-49.91	27.5	8.1
2012/04/11 08:39:31.4	92.82	2.35	45.6	8.6
2012/04/11 10:43:38.2	92.31	0.90	54.7	8.2

Table 2. Teleseismic earthquakes in this study

#	Date	Longitude	Latitude	Depth	Mw	H17A	SRU	SDCO
1.	2004/12/23 14:59:30.9	161.25	-49.91	27.5	8.1	N/A	x	N/A
2.	2004/12/26 01:01:09.0	94.26	3.09	28.6	9.0	N/A	x	x
3.	2005/03/28 16:10:31.5	97.07	1.67	25.8	8.6	N/A	N/A	x
4.	2006/04/20 23:25:17.6	167.05	60.89	12.0	7.6	N/A	x	x
5.	2006/05/03 15:27:03.7	-173.47	-20.39	67.8	8.0	N/A	N/A	x
6.	2006/11/15 11:15:08.0	154.33	46.71	13.5	8.3	N/A	x	x
7.	2007/01/13 04:23:48.1	154.8	46.17	12.0	8.1	N/A	x	x
8.	2007/04/01 20:40:38.9	156.34	-7.79	14.1	8.1	N/A	Yes	x
9.	**2007/08/15 23:41:57.9**	**-77.04**	**-13.73**	**33.8**	**8.0**	N/A	**Yes**	x
10.	**2007/09/12 11:11:15.6**	**100.99**	**-3.78**	**24.4**	**8.5**	N/A	**Yes**	x
11.	2007/11/14 15:41:11.2	-70.62	-22.64	37.6	7.7	x	x	x
12.	**2008/05/12 06:28:40.4**	**104.10**	**31.44**	**12.8**	**7.9**	**Yes**	x	x
13.	**2009/05/28 08:25:04.8**	**-87.17**	**16.5**	**29.0**	**7.3**	x	**Yes**	x
14.	**2009/09/29 17:48:26.8**	**-171.97**	**-15.13**	**18.5**	**8.1**	x	**Yes**	x

15.	**2009/10/07 22:19:15.3**	**166.01**	**-11.86**	**41.7**	**7.8**	x	**Yes**	x
16.	2010/02/27 06:34:13.0	-72.93	-36.15	28.1	8.8	x	x	x
17.	2010/04/04 22:41:09.2	-115.39	32.31	12.8	7.2	x	x	x
18.	2011/03/11 05:47:32.8	143.05	37.52	20.0	9.1	x	x	x
19.	2011/06/24 03:09:51.5	-171.77	52.09	74.2	7.3	x	x	x
20.	**2012/03/20 18:02:54.9**	**-98.39**	**16.6**	**15.4**	**7.5**	**Yes**	x	x
21.	**2012/04/11 08:39:31.4**	**92.82**	**2.35**	**45.6**	**8.6**	**Yes**	**Yes**	**Yes**
22.	2012/04/12 07:16:04.6	-112.76	28.57	15.8	7.0	x	x	x
23.	**2012/08/27 04:34:39.5**	**-89.17**	**12.02**	**12.0**	**7.3**	x	Yes	**Yes**
24.	**2012/09/05 14:42:23.3**	**-85.64**	**10.00**	**29.7**	**7.6**	x	**Yes**	Yes
25.	2012/10/28 03:04:37.2	-132.06	52.61	12.0	7.8	x	x	x
26.	2012/11/07 16:35:56.3	-92.43	14.11	21.3	7.4	x	Yes	x
27.	2013/01/05 08:58:31.5	-134.97	55.69	13.8	7.5	x	N/A	x
28.	2013/02/06 01:12:55.0	165.21	-11.18	20.2	7.9	x	x	x
29.	2014/04/01 23:47:31.5	-70.81	-19.70	21.6	8.1	x	x	x
30.	**2014/04/03 02:43:35.9**	**-70.6**	**-20.43**	**28.7**	**7.7**	x	**Yes**	x
31.	2014/04/18 14:27:36.0	-101.25	17.55	18.9	7.3	x	N/A	x
32.	2014/10/14 03:51:43.7	-88.45	12.33	40.8	7.3	x	x	x
33.	2015/09/16 22:55:22.9	-72.09	-31.13	17.4	8.3	x	x	x
34.	2016/04/16 23:58:57.0	-80.25	-0.12	22.3	7.8	x	Yes	x
35.	2016/12/17 10:51:56.3	153.76	-5.55	52.8	7.9	x	x	x
36.	2017/07/17 23:34:57.7	169.78	54.13	23.2	7.7	x	x	x

37.	**2017/09/08 04:49:44.2**	**-94.62**	**15.34**	**50.2**	**8.2**	**Yes**	x	x
38.	2017/09/19 18:14:47.1	-98.62	18.51	52.7	7.1	x	x	x

*Note: Yellowstone (H17A station) recorded tremor, and Utah (SRU station) and Colorado (SDCO station) recorded triggered earthquakes.

* **Yes**: triggered event (recorded by more than one station); x: non-triggered event; N/A: no data available.

*Units: longitude and latitude is degree; depth is km.

Table 3. Possible triggered earthquakes were recorded by station H17A (near Yellowstone) and nearby stations.

#	Date	Stations
12.	2008/05/12 06:28:40.4	H17A
20.	2012/03/20 18:02:54.9	H17A, B944
21.	2012/04/11 08:39:31.4	H17A
37.	2017/09/08 04:49:44.2	H17A

Table 4. Possible triggered earthquakes were recorded by station SRU (central Utah) and nearby stations.

#	Date	Stations
8.	2007/04/01 20:40:38.9	SRU
9.	2007/08/15 23:41:57.9	SRU, P14A, Q14A, P16A, Q16A, P17A, R17A, Q18A

10.	2007/09/12 11:11:15.6	SRU, TMU, Q18A, Q16A, P18A, ROA, P17A, DBD
13.	2009/05/28 08:25:04.8	SRU, Q16A, P18A, S18A, P19A, O19A, DUG, Q20A, R20A, O20A, S20A, N20A, N21A, N22A, R24A
14.	2009/09/29 17:48:26.8	SRU, CCUT, Q16A, R11A
15.	2009/10/07 22:19:15.3	SRU, Q16A
21.	2012/04/11 08:39:31.4	SRU, TMU, CVRU, BCE, PNSU, ROA, DCM, ARGU
23.	2012/08/27 04:34:39.5	SRU, TMU
24.	2012/09/05 14:42:23.3	SRU, ARGU, DCM, PNSU
26.	2012/11/07 16:35:56.3	SRU
30.	2014/04/03 02:43:35.9	SRU, ARGU, CVRU, BCE, ROA, BCW, DCM, TMU, EMU, SNO
31.	2014/04/18 14:27:36.0	ARGU, DCM, EMU
34.	2016/04/16 23:58:57.0	SRU

Table 5. Possible triggered earthquakes were recorded by station SDCO (near Raton Basin) and nearby stations.

#	Date	Stations
21.	2012/04/11 08:39:31.4	SDCO, T25A, Q24A, S22A, XTOCO, HGTCO, LVTCO
23.	2012/08/27 04:34:39.5	SDCO, T25A, S22A, Q24A, ANMO, TASL, TASM, KSCO, MVCO, ISCO, AMTX, MSTX, CBKS, OGNE, SRU, MNTX, WMOK
24.	2012/09/05 14:42:23.3	SDCO